

Ocean wave dynamics in the coastal area of the central west coast of India and its variability

P. Aravind, M.M.Amrutha, V. Sanil Kumar*

Ocean Engineering Division, CSIR-National Institute of Oceanography, Goa - 403004 India

*Corresponding author email: sanil@nio.org; Tel: 0091 832 2450327

Abstract

Examined the spatial and temporal changes in the wave spectra using waves measured in the coastal area at two locations for three years. Long-term variability is examined with ERA5 reanalysis data. The annual average wave spectra have a significant wave height (H_s) of ~1m at both locations. During the Asian monsoon (June-September), the highest wave spectra resulted in H_s of 5.1m. Frequently, the wave pattern is with H_s of 0.4-0.8m and mean period of 3-8s. Annually, ~67% of the time, spectra consists of waves from 210-230°, 250- 260°, and 300-310° with high waves ($H_s > 4m$) from southwest (250-260°). Due to the presence of significant wind-seas and swells, energy at the secondary spectral peak is ~38% of energy at the principal peak. During February-May, the sea state is dominated (~50% of time) by locally generated waves and young swells, while in monsoon, the swells are large (66-75%). Principal component (PC) of spectral energy density shows that monsoon and cyclonic storms are resulting in a large variability (~90%) in the first mode. Even though the wave characteristics are similar within 125km distance, some metrological events cause significant changes in the waves and it resulted in different 100-year return period values at these locations.

Keywords: Extreme waves, Long-term variability, Multi-peaked wave spectrum, Reflected waves, Wind-generated waves

1. Introduction

The surface waves generated by winds (waves, hereafter) play an important role in many scientific and practical studies. Waves in the coastal waters significantly impact surf zone circulation and coastal erosion (Thornton and Guza, 1986). In addition, the primary mechanism for sediment transport and mixing in the coastal zone are the wave-driven processes and these processes depend on the energy and direction of the incident waves (Masselink and Pattiaratchi, 2001). The waves in the ocean consist of locally generated waves (wind-sea, which are short-period/high-frequency) and the waves generated far off (swells, which are long-period/low-frequency). Hence, the wave spectrum measured at a location in the ocean will be the sum of many wave components produced by winds separated in space and time. The swells can propagate great distances away from their source (Sverdrup and Munk, 1947), and hence, the wave-field at a location generally will be a result of both the local and remote forcing (Alves, 2006; Semedo et al., 2011; Rueda et al., 2017). The swells can be classified based on significant wave steepness [ratio of significant wave height (H_s) and wavelength (L)] and the distance to the generation area: "young" ($0.01 \leq H_s/L < 0.025$), "mature" ($0.004 \leq H_s/L < 0.01$) and "old" ($H_s/L < 0.004$). The safety hazards associated with swells and wind-sea components differ, and hence it is important to differentiate between the two (Chawla et al., 2013). Due to the combined existence of swells and wind-seas, the wave spectra are generally bimodal. For example, in southern California, 50% of the sea states are bimodal (Crosby et al., 2016). The spectra with the bimodal structure are ~20 to 25% in the North Atlantic (Soares, 1991). Annually off the southern Brazilian coast, 31% of the spectra are multi-peaked (Cuchiara et al., 2009). In the Indian coastal waters, ~60% of the spectra are multi-peaked (Kumar et al., 2003). In the surf zone, wave reflection from very steep beaches is up to 60% for long-period waves (Elgar et al., 1994) and causes multi-modal spectra.

Multi-modal waves cannot be properly defined with integrated parameters. Hence, the wave spectrum depicting how spectral energy density is scattered over directions and frequencies are to be used to categorize different wave systems. The shortcomings of using bulk wave parameters for the characterization of waves for many regions of the world are reported by Portilla et al. (2016). Many studies use the wave direction of the largest energy peak of a spectrum, which leads to potentially misleading longshore sediment transport (George et al., 2020) in areas where significant energy is present in secondary spectral peaks. Defining the peak wave period (T_p) and mean wave direction in a case with swells and wind-seas will only consider the most energetic one and disregard the other.

Oceanographic conditions of the nearshore waters along the eastern Arabian Sea (AS) are subjected to seasonal variability. The AS experiences three different seasons: pre-monsoon (February-May), Asian monsoon/summer/southwest monsoon (June-September) and northeast monsoon (October - January). The southwest (SW) monsoon winds are stronger and pre-monsoon and northeast (NE) monsoon winds are generally weak. Accordingly, the wave climate in the region is affected by the prevailing southwest winds, swells propagating from the south-southwest and the northwest winds (Glejin et al., 2013; Kumar et al., 2014; Anoop et al., 2015; Amrutha et al., 2017; Anoop et al., 2020; George et al., 2020). The central west coast of India is in the tropical zone and hence the ocean is dominated by swells all year round. Due to the swell domination, most of the spectral energy is in the low-frequency part (Anjali Nair and Sanil Kumar, 2017). While swells originated in the South Indian Ocean and the Southern Ocean are a major source of wave variability in the eastern AS (Alves, 2006; Naseef and Kumar, 2020), their energy gets dissipated on the way, resulting in small significant wave heights. In shallow water, nonlinear triad wave-wave interactions and wave dissipation by interactions with the bottom becomes crucial.

Wave statistics of the Indian coastal waters are documented by Chandramohan et al. (1991) based on ship reported deep-water wave data. The wave climate studies gain momentum after the establishment of directional wave rider buoys at various coastal locations in the shelf sea of India (e.g., Kumar et al., 1999; 2003; Kumar and Anand, 2004; Aboobacker et al., 2011a; Glejin et al., 2013; Kumar et al., 2014; 2019). Even though the coastal waters of the eastern AS are subjected to similar open sea conditions, annually the percentage of multi-peaked wave spectra varied largely within 350 km; 54% in the north to 37% in the south, because of the variation in local winds (Kumar et al., 2014). Understanding the spatial and temporal variability of wave climates is essential for ensuring robust coastal management in the future (Harvey and Woodroffe, 2008). The changes in the wave conditions are other major concerns for the nearshore and offshore industries. Understanding the wave energy from different directional sectors is less understood in the coastal areas off the central west coast of India. High tides coinciding with southwest monsoon storm waves can also flood the coastal areas, especially low-lying areas.

The lack of wave data covering different years in the nearshore areas poses challenges to the coastal engineers. Hence, they are forced to depend on numerical models or data from nearby areas. Computational costs limited the global operational model to a grid of $1^\circ \times 1^\circ$ to $1.5^\circ \times 1.5^\circ$ and $0.25^\circ \times 0.25^\circ$ for regional models (Chawla et al., 2013). Thus, it is crucial to assess the variations in wave characteristics from place to place within 1 to 1.5° , which is one of the objectives of this paper. To

study the coastal hydrodynamics and nearshore developments, waves measured in the nearshore are required. By using field observations of waves and reanalysis data, this paper examines the spatial and temporal variations in wave parameters at two locations off the west coast of India spaced at ~125 km (~1.13°) along the eastern AS. Since the changes in bathymetry cause wave refraction, focusing or spreading wave energy (e.g., Ardhuin et al., 2003), the wave data at the same depth contour (~ 15 m water depth) are used in the study. Since during the southwest monsoon, in the eastern AS waves break in water depth less than 10 m, buoys are deployed at 15 m water depth. Apart from assessing the variability of wave height, period, direction and wave spectra at the two locations, we examined; i) if swells propagating from the Southern Ocean heavily influences the local wave climate at the central west coast of India; ii) the seasonal change of wave spectra, especially the differences of wave conditions between southwest monsoon season and the other seasons in one year. Since there is a lack of long-term measured wave data for the eastern AS, the long-term variations in wave height is studied based on 28 years (1992 to 2019) of hourly reanalysis data of significant height and maximum wave height.

The paper is organized as the following: Section 2 describes the study area, data and methods used in this investigation. In section 3, the obtained results are presented and discussed. Section 4 presents the conclusions of the study.

2. Data and methods

2.1 Study area

Wave data measured at 2 locations; Vengurla (15.842° N; 73.563° E) and Karwar (14.822° N; 74.052° E) spaced at ~ 125 km along the eastern AS (Fig. 1) with the directional waverider buoy, for three years (1 January 2015 to 31 December 2017) is used in the study. By analysing the wave spectral characteristics at Karwar from 2011 to 2015, Anjali Nair and Sanil Kumar (2017) reported that the measured spectra are represented by JONSWAP spectra (Hasselmann et al., 1973) at low frequencies and Donelan spectra (Donelan et al., 1985) at high frequencies with modified spectral parameters. Tides in the study region are mainly semi-diurnal. The average tidal range at the northern location (Vengurla) and the southern location (Karwar) is about 2 m during the spring tide. In comparison, the tidal range is about 0.6 m at the northern location and is about 0.8 m at the southern location during the neap tide. It is the region of heavy rainfall with an average rainfall of about 300 cm in a year. The continental shelf of the study region is comparatively wide, with 50 m depth occurring at 35 km, 100 m at 80 km away from the coast.

2.2 Buoy data

At each location, 0.9 m diameter Datawell MKIII directional waverider buoy (Datawell, 2009) was moored with the standard mooring and the data was collected for 3 years. The three accelerometers; one vertical and two horizontal directions oriented orthogonally are measured and converted into translational motions in the respective direction. In the internal memory of the buoy, all the 3 translational motions are stored and retrieved later during the annual maintenance. Every 30 minutes data are processed as one record, whereas the displacement of the buoy is recorded with a sampling interval of 0.78125s during the measurement period. Due to the drifting of the deployed buoy from the moored location at Karwar and retrieval of wave buoys for routine maintenance, 100% data could not be collected in all the years at both locations. A pronounced peak of the spectral density at the low-frequency side of the spectrum raises the suspicion that the stabilized platform suspension is out of order and can be spurious data (Datawell, 2009). Checked for spectral peaks that are orders of magnitude higher than $10^{-2} \text{ m}^2 \text{ Hz}$ in the frequency range (0.025-0.035 Hz) and found that such peaks are present in few records and these data are not used in further analysis. The data used in the analysis are 85, 96.5 and 99.5% at Karwar and 99.9, 96 and 100% at Vengurla in the years 2015, 2016 and 2017.

Wave data analysis is carried out both in the frequency and time domain. Wave spectrum is obtained from the fast Fourier transform of eight series, each consisting of 256 data points (Datawell, 2009). Significant wave height (H_s) and the mean wave period (T_{m02}) are calculated from the wave spectral moment. More details on the data analysis are available in Kumar et al. (2014). Wave spectrum with frequency ranging from 0.025 to 0.58 Hz is considered in the wave data analysis. The frequency resolution is 0.005 Hz for frequencies less than 0.1 Hz and it is 0.01 Hz from 0.1 to 0.58 Hz. T_p and mean wave direction (θ_m) corresponds to the peak of the wave spectral energy density of the sea surface height. The directional spread and wave direction are calculated following the circular moments (Kuik et al., 1988). From the half-hourly wave spectrum, the monthly and seasonally averaged wave spectrum is obtained by averaging the spectral energy density at the respective frequencies over the specified time interval. The time referred to in this article is the Coordinated Universal Time (UTC). The role of long-period waves ($T_p > 12 \text{ s}$), short-period waves ($T_p \leq 6 \text{ s}$) and intermediate period waves ($6 < T_p \leq 12 \text{ s}$) in the measured wave data is also evaluated. The direction represents where the waves come from; 0° means waves are coming from the north, 90° waves from the east, and so on.

To provide a better description of the waves in the study region, the wave spectra are analyzed individually and characterized by the dominance of wind-sea or swell. The directional spectrum, $E(f, \theta)$ is partitioned into wind-seas ($f_1=f_c$, $f_2=0.58$ Hz) and swells ($f_1=0.025$, $f_2=f_c$) and each of them is further partitioned into four components as per equation 1 based on the direction of approach (θ); $0-168^\circ$ represents reflected waves from the coast and/or the waves due to sea breeze, $168-248^\circ$ represents waves from southern ocean/Indian Ocean, $248-276^\circ$ represents the waves from southwest-west and $276-360^\circ$, the northwest-north waves. f_c is the separation frequency estimated following Portilla et al. (2009). The wave parameters at 2 locations are inter-compared using the bias (BIAS), the root-mean-square error (RMSE), the correlation coefficient (R), and the scatter index (SI).

$$H_{s_1} = 4 \sqrt{\int_{f_1}^{f_2} \int_{\theta_1}^{\theta_2} E(f, \theta) df d\theta} \quad (1)$$

For finding the variability of spectral energy density, Empirical Orthogonal Function (EOF) analysis is carried out. EOF analysis is performed to find out the spatial and temporal variability patterns of a variable (e.g., Preisendorfer and Mobley, 1988). For this study, we addressed the difference in the inter-seasonal variation of the spectral energy density of waves at Vengurla and Karwar. EOF is performed on multi-dimensional climate variables $Z(x,t)$, where x is the vector space and t is the time. EOF is mainly eigenvectors of covariance matrix containing different modes. The first mode gives the largest variability and the subsequent modes give the next largest ones. Very few studies approach one dimensional (1-D) EOF method, which predicts the time series (Principal component) variation of variables (e.g., Tolkova, 2010). Similarly, we also performed a time series analysis (PC) of spectral energy using EOF.

2.3 Reanalysis data

Reanalysis ERA5 data used in the study were obtained from the European Centre for Medium-Range Weather Forecasts (ECMWF) with a resolution of $0.5^\circ \times 0.5^\circ$ (Hersbach et al. 2020). Even though ERA5 wave heights are compared with buoy-measured data for various locations in the north Indian Ocean (Naseef and Kumar, 2020), the ERA5 H_s and H_{max} data for the study locations are compared with the measured buoy data from 2015 to 2017 (Fig. 2). The parameters used for comparison of the data are the root-mean-square error (RMSE), correlation coefficient (r), and bias. The bias signifies the average difference between the ERA5 and buoy data and low RMSE values indicate a better fit of ERA5 data with measurements. The correlation coefficient 0.98 for H_s and

0.97 for H_{\max} at both locations. The bias is positive and varies from 0.08 m to 0.18 m for H_s and 0.55 m to 0.67 m for H_{\max} . Positive bias indicates a higher wave height in ERA5. Since the ERA5 data grid point is a comparatively deeper water depth than the buoy location, ERA5 wave height data is higher than the buoy data. The measured buoy data is a point measurement, whereas the ERA5 data were produced on a grid with a resolution of the order of 31 km and the mean water depth at the point of interest is different from the buoy location. But the wave direction in the ERA5 data has a large deviation from the measured buoy data in the coastal waters (Fig. 2). Buoy mean wave direction corresponds to the spectral peak and in the study area, most of the time significant differences are reported in the direction of wind-seas and swells (Amrutha et al., 2016). So when wind-seas and swells co-exist with almost equal magnitude, a large difference can be observed between ERA5 and buoy data.

2.4 Numerical wave model

WAVEWATCH-III (WWIII) numerical model version 4.18 (Tolman, 1991) developed at NOAA/NCEP (National Centres for Environmental Prediction) is used for the simulation of waves. The simulations are carried out for the year 2015. Two model domains are considered, i) a big domain (75°S - 35°N & 20°E - 112°E) with a resolution of 0.5° covering the entire Indian Ocean and part of the Southern Ocean and ii) a small domain (5°N - 25°N & 60°E - 90°E) with a resolution of 0.1° . The model is forced with ECMWF ERA5 wind with 1-h resolution and bathymetry data used is from ETOPO1 (Amante and Eakins, 2008). The spectrum has 36 directional bins and 25 frequency bins spaced exponentially from 0.04 to 0.4056 Hz. Further details of the model setup and the model validation with buoy measured wave data are described in Amrutha et al. (2016). Among different parametrizations, ST4 physics showed the best performance for a location in the eastern AS and hence in the present simulations also ST4 physics is used. The wave spectrum obtained from the model is compared with the buoy data of Vengurla and Karwar.

2.5 Storms and cyclones during 2015-2017

During the measurement period, a number of cyclones formed in the AS (Table 1). A brief description about all storm and cyclones occurred in AS from 2015 to 2017 is presented here and the track of the cyclones are presented in Fig. 1. A low-pressure area formed at 14.5°N , 68.5°E on 6 June 2015 developed into TC Ashobaa on 7 June 2015 and attained a peak intensity of 23 m/s and moved towards the Oman coast (Fig. 1). A depression formed at 11.5°N , 65°E on 28 October in central AS developed as cyclonic storm Chapala on 29 October 2015 and moved towards western AS. On 30 October TC attained a peak three-minute sustained winds of ~ 59 m/s (IMD, 2016). TC

Megh was formed on 5 November 2015 at east-central AS (14.1° N, 66° E) followed a path similar to Chapala with a peak intensity of ~ 49 m/s. After moving northward, the cyclone turned to the west, thereafter, the cyclone crossed the Yemen coast. TC Ockhi originated in the eastern Andaman Sea on 21 November 2017 and dissipated near the south coast of Gujarat on 6 December 2017 (IMD, 2017).

2.6 Extreme wave analysis

Extreme value analysis is carried out by following the Generalized Extreme Value (GEV) Distribution model with annual maximum values (Goda, 1992). Estimate based on annual maximum values is the common approach to ensure that the dataset truly represents extreme values and that the data are independent (Takbashi and Young, 2019).

3. Results and discussions

3.1 Intra-annual variability in wave spectral parameters

The time series plot of H_s at Vengurla and Karwar from 1 January 2015 to 31 December 2017 indicates that the pattern of variation is similar at both locations (Fig. 3). As seen in Figure 3, the overall variability of H_s is distinct by an annual cycle that peaks in the southwest monsoon, with H_s of 5.1 m. The maximum H_s of ~ 5.1 m is in 2015 at both locations, whereas it is 4.2 m at Vengurla and 3.8 m at Karwar in other years. This noticeable change in the year 2015 is mainly due to the influence of tropical cyclone (TC) Ashobaa (7-12 June) occurred in the northern AS (Kotal et al., 2016). The list of TCs formed in the AS from 2015 to 2017 is listed in Table 1. In December 2017 the value H_s is about ~ 2.5 m in both locations, whereas in 2015 and 2016, it is less than 2 m. This significant change in H_s in 2017 is due to the impact of TC Ockhi (28 November – 6 December). Kumar et al. (2018) observed similar changes in waves at 370 km north of Vengurla during TC Ockhi. Even though the locations Karwar and Vengurla are ~ 125 km apart, the high waves occurred almost simultaneously at both locations (Figs. 3a and 3b). The distribution of H_s in different height ranges indicates that the predominant wave height ranges are 0.4 to 0.8 m (Fig. 4a) with mean periods of 3 to 8 s with occurrences of 45 and 49% at Karwar and Vengurla. Abnormality index i.e., the ratio of maximum wave height to significant wave height in a record, indicates that only 3% of the records in the analyzed dataset contained freak (rogue) waves. Although the number of freak waves was small, all of them were with H_s higher than 1 m (Figs. 4d and 4e).

A large variation in the magnitude of T_p is observed due to the combined presence of swells and wind-seas in the pre-monsoon and northeast monsoon periods (Figs. 3c and 3d). The longer-period waves that are seen in Figure 4 in the non-monsoon period are a great example of the swell

dominance in the study area. The T_p of 10 to 14 s is most frequent with 52 and 56% at Karwar and Vengurla (Fig. 4b). The waves are predominantly (during 43% and 41% at Karwar and Vengurla) from 210° to 230° . Waves are from 250° to 260° during 17% and 19% of the time at Karwar and Vengurla and are from 300° to 310° during 8 and 6% of the time at Karwar and Vengurla (Fig. 4c).

The joint distribution of significant wave height and T_p indicates that the most frequent (45 to 48%) wave pattern for the southwest monsoon is with H_s 1.6 to 2.4 m and T_p 10 to 12 s. Throughout the northeast monsoon, an increase in the period is observed, located between 12 and 16 s, though the H_s (0.4 to 0.8 m) has been the same as in the pre-monsoon (Table 2). Also, there are relatively larger (20-30%) short-period waves (4 to 6 s) in the pre and northeast monsoon. The highest waves for each season are as follows: 7.9 m, with a period of 12 s for the southwest monsoon; 3.9 m, with a period of 8.5 s for pre-monsoon; and 3.1 m, with a period of 7 s for northeast monsoon. All these waves had their direction from W-SW, with the one from northeast monsoon coming from S-SW.

The monthly mean wave parameters (H_s , mean wave period, T_p , wavelength, percentage of swell and mean wave direction) show a qualitatively close agreement between the two stations (Fig. 5). H_s and mean wave period is relatively higher at Karwar than Vengurla and the estimated difference in these parameters at the locations ~125 km apart are about 10–15%. At Karwar, the monthly average H_s ranges from a maximum of 2.3 m in June and July and a minimum of 0.6 m from November to January, whereas at Vengurla, it varied from 2.1 to 0.5 (Fig. 3). In line with earlier studies (e.g., Anoop et al., 2015; Naseef and Kumar, 2020), the Findlater jet (Findlater, 1969) is found to have a strong influence on the southwest monsoon-averaged H_s . The high H_s in June–July is due to the intense southwesterly swell, mainly generated by the Findlater jet. Wave height in the most energetic months can be up to a factor 3.9 greater than in the calmer months (Fig. 3).

One might hypothesize that the Southern Ocean swells that propagates all the way to the west coast of India. To investigate this hypothesis, we present the wave rose diagram of H_s for measurements in different months at Vengurla (Fig. 6). From June to August during the southwest monsoon, the distributions are predominantly narrow, with most waves from the SW to W (240 – 270°), with H_s from 1.5 to 5 m, and T_p from 10 to 14 s (Fig. 6). In February–April, the pattern is rather different with waves mostly from the northwest (290 – 320°). Even though the remotely generated southern swell (180 – 225°) is relatively frequent (~73%), in October–November, the majority of the waves with $H_s > 1$ m. The wave rose diagram of T_p (Fig. 6), indicates that the northwest waves have a slightly shorter period ($T_p < 8$ s), which implies that they are locally

generated waves or young swells. The locally-generated wind waves and young swells are forced by regional-scale wind events that occur in the directional sector between 290° and 320° .

From a seasonal perspective, significant variations are observed in all wave properties in the study area. During the southwest monsoon, most of the waves (88%) are young swells or wind-seas, 11.6% are mature swells and only 0.3% are old swells. While in the northeast monsoon, 50% of the waves are old swells, 34% are mature swells and 16% are young swells and wind-seas. During pre-monsoon 18% are old swells, 51% are mature swells and 31% are young swells and wind-seas. During the southwest monsoon, waves from SW-W ($240-270^\circ$) dominate the data set, with 86 and 91% of the occurrence at Karwar and Vengurla (Fig. 6). That scenario modifies in northeast monsoon, with a direction switch of the waves from S-SW ($210-230^\circ$) with frequencies of 61 and 64% at the locations. During pre-monsoon, wave characteristics are similar to that of the northeast monsoon, with the most frequent waves from S-SW, with 54 and 51%, respectively, at Karwar and Vengurla along with waves from NW ($290-310^\circ$).

The annual wave rose diagram at Karwar and Vengurla indicates changes in the northwesterly waves are relatively less at Vengurla (Fig. 6). The study shows that throughout the year, swells generated by westerlies in the southern hemisphere can propagate into the study area similar to the earlier observations for locations in the eastern AS (Amrutha et al., 2017) while waves due to intertropical convergence zone induced easterly trade winds and Somali jet (Findlater, 1969) are present during June-September.

3.2 Wave spectrum

The spectral analysis decomposes the chaotic surface waves into linear waves having different heights, directions and frequencies. There is a low-frequency signal in the study area that is present throughout the year with varying intensities (Fig. 7). These low-frequency waves correspond to the south Indian Ocean and the Southern Ocean generated swells (Naseef and Kumar, 2020), which is more intense in June–July–August months (Fig. 7). There is a high-frequency component that shifts its direction during the year. The high-frequency signal is mainly northwesterly during December-April and southwesterly in June-August, which is directly related to the trade winds. The waves dominated by local seas, i.e., short-period waves (wave period < 6 s) in the measured data of the surface height variance is 18-59% and a relatively high percentage is seen in December-April due to the enhancement in the local winds with the maximum in February (Fig. 8). The northwesterly waves are mainly due to Shamal and Makran events (Aboobacker et al., 2011b; Anoop et al., 2020).

The evaluation of the wave spectrum obtained from the numerical model WWIII is done by comparing the monthly average wave spectra with buoy data of Vengurla and Karwar for 2015 (Fig. 9). It is observed that in all months, the numerical model over predicts the swell part at Vengurla, while at Karwar, the numerical model slightly underestimated the swell peak except in February and November. At both locations, from January to May, when considerable wind-seas are present, the model under predicts the wind-sea part. The input wind data used is the ERA5, the resolution of which (~31 km) is not sufficient in the coastal areas subject to sea breeze/land breeze and local wind systems. In addition, the orographic effects and bathymetry play important role in the nearshore environment (within 5 km from the coast), where the measurements are done.

The annual mean wave spectrum for different years is displayed in Fig. 10. The local peaks in a wave spectrum represent various meteorological characteristics. There are two predominant energy peaks at 0.077 Hz, 220° and 0.20 Hz, 290°, which correspond to two predominant wave climate systems. In a year, during 12.2% of the time, which is mainly in the non-monsoon period, the spectral energy of the wind-sea peak is 1.8 times that of the swell. The remaining time of the year (87.8%), on average, spectral energy at the wind-sea peak is one-third of that at the swell. The presence of significant wind-seas and swells causes a multi-peak spectrum with large spectral energy at both peaks. At the secondary spectral peak, the spectral energy is ~38% of that at the primary peak. During February-May, the sea state off the central west coast is dominated (up to 50% of the time) by the short period, locally generated waves. In contrast, during the southwest monsoon, the percentages of swells are large (66 to 75%).

Annual average directional spectra show the two well-separated wave systems; southwesterly swells and northwesterly wind-seas (Fig. 10). Annually the wave spectra are single-peaked during 39.4 to 43.6% and are maximum during the southwest monsoon period and are minimum in March-April during which the multi-peaked wave spectra are maximum (Table 3). Most of the multi-peaked and single-peaked wave spectra are swell-dominated. For a location in the eastern AS, 130 km north of Vengurla, Anjali et al. (2016) observed that over an annual cycle, 29 % of the wave spectra are single-peaked swell spectra and 42 % are multi-peaked swell spectra.

In a year, on average, 26% of the sea surface height variance is a result of wind-seas from 280° to 360° and 28% are the swells from the southwest (168-248°) (Fig. 11). In a year, 8% are wind-seas and 16% are the swells from the directional sector 248° to 280° (Table 4). 4% of the sea surface height is the swells from 280° to 360° and 9% are the wind-seas from 168° to 248°. The waves from 0° to 168° are the waves from the coastal direction and in a year, these waves contribute ~9% of the

sea surface height variance (Fig. 11). The waves from the coastal direction are partly due to the reflected waves and partly are the waves due to land breeze (Anoop et al., 2014). Seasonally significant variations are observed in both the swell and wind-sea contribution to the sea surface height variance from different directional sectors (Table 4).

From February to May, the northwesterly wind-seas and young swells (significant wave steepness from 0.1 to 0.025) is 35 to 41% at Vengurla and 30 to 47% at Karwar (Table 4). Aboobacker et al. (2011b) reported the presence of summer shamal waves in the eastern AS during the pre-monsoon period. Northwesterly wind-seas and young swells are also significant from October to January (29 to 33% at Vengurla and 30 to 33% at Karwar) (Table 4). Anoop et al. (2020) reported that the presence of makran winds and the associated waves in the northern AS during the northeast monsoon and pre-monsoon seasons (October–May). These northwesterly waves with period less than 8s are mainly due to the shamal and the makran winds. No significant variation is observed in the northwesterly waves at the two locations studied. During the pre-monsoon and northeast monsoon period, young swells are mainly from the northwest, while the mature and old swells are from the southwest (Fig. 12). During the southwest monsoon, young swells are from the west and matured and old swells are from the southwest.

Figure 13 shows the percentage of long-period (wave period > 12 s), intermediate-period and short-period waves in different months at Vengurla and Karwar. The contribution of long-period swells in the wave spectral energy is least in June (~8%). The intermediate-period waves ($6 \text{ s} \leq \text{wave period} \leq 12 \text{ s}$) are high (62 to 69%) from June to September due to the influence of the southwest monsoon (Fig. 13). At both locations, the variations in the percentage of different types of waves are similar. At the northern location (Vengurla), slightly higher (~7%) long-period waves are observed compared to the southern location (Karwar), whereas the intermediate and short-period waves are higher in the southern location. The mean energy wave period, T_{m-10} , gives extra weight to the lower frequencies, and therefore to the longer period waves in the spectrum than mean wave periods T_{m02} . T_{m-10} is higher (~8.5 s) during the southwest monsoon and northeast monsoon months, indicating large longer period waves compared to pre-monsoon months.

PC of the spectral density of waves at Vengurla and Karwar for the year 2017 indicates that the first mode shows strong variability (84% and 80%) mainly in the southwest monsoon period in both regions with the same pattern (Fig. 14). There is also a peak in November and December that shows the influence of severe TC Ockhi, which formed in the AS. All the TCs formed in the AS from 2015 to 2017 are presented in Table 1. In the second mode, Karwar shows more variability

(9.2%) than Vengurla (6.34%) due to the geographical position of these two regions (Karwar below Vengurla). During the end of November and at the beginning of December, the influence of TC Ockhi is clearly seen in PC2 and PC3. The influence of the sea breeze from January to May is seen in PC2 and PC3.

PC of half-hourly variability at Vengurla in 2015 and 2017 (Fig. 14) indicates that the first mode variability in 2015 is more than (90%) that of 2017 (84%). Southwest monsoon is the dominant factor of both years. In 2015, a cyclonic storm Ashobaa formed in the AS from June 7 to 12 (Kotal et al., 2016) and made landfall at the Oman coast; this also caused the large variability in 2015. The second mode is (6.34 % and 8.2%) opposite to that of the first mode, which is mainly due to the influence of TC Ockhi formed in AS from 28 Nov to 6 Dec 2017 (IMD Report, 2017).

Directional spreading is narrowest at the spectral peak (f_p) and broadened at frequencies higher and lower than f_p . The directional spreading parameter for high waves ($H_s > 3$ m) is less with an average value of 18° compared to the annual average of 25° . In the region of the spectral peak (peak frequency) of the wave spectrum, the components are unimodal, and the number of bimodal distributions increases at both above and below the peak frequencies similar to the observations of Young et al. (1995). The observed directional spread at the peak frequency for swell is about 10° , while for wind-sea; it is 30° (Forristall and Ewans, 1998).

3.3 Long-term variations in wave height

The wave climate at Vengurla from 1992 to 2019 is characterized by annual mean H_s of 1.19 m and that of Karwar is 1.24 m. Maximum H_s during 1992-2019 is 5.06 m at Vengurla and 5.19 m at Karwar. While the annual mean H_{max} is 2.22 m and 2.34 m at Vengurla and Karwar with a maximum height of 9.18 m and 9.88 m at Karwar. At Karwar, the highest H_s (5.19 m) and H_{max} of 9.88 m were on 29 May 2006 and the next highest value (H_s of 5.18 m and H_{max} of 9.56 m) was on 17 June 1996. On 29 May 2006, the directional waverider buoy deployed at 14 m water depth off Goa, a location ~ 72 km north of Karwar recorded H_s of 5.65 m and H_{max} of 8 m (Kumar et al., 2010). At Vengurla, the highest H_s (5.06 m) and H_{max} of 9.18 m was on 18 June 1996. A depression developed on 17 June 1996 developed into a severe cyclonic storm ARB 01 on 18 June 1996 caused the highest wave heights at Karwar and Vengurla. The buoy measured H_s and H_{max} at 23 m water depth at allocation between Karwar and Vengurla (~ 75 km north of Karwar) is 5.9 m and 10.1 m (Kumar, 2006).

Even though Vengurla and Karwar are located within 125 km and are in the Open Ocean, there is a large variation in wave height on 29 May 2006. During one such event from 29 May 2006

2100 hrs to 30 May 2006 0000 hrs, the maximum H_s at Karwar is 5.19 m, while that at Vengurla is only 3.05 m. Similarly, during this period, the maximum H_{max} is 9.88 m at Karwar and is 5.63 m at Vengurla. Snapshot of H_s during 29 May 2006 2100 hrs to 30 May 2006 0000 hrs shows the variation in wave height along the eastern AS (Fig. 15).

Since there are significant variations in wave heights at Vengurla and Karwar for some metrological events as seen during 29-30 May 2006, there is significant variation in 100-year return period wave height at these two study locations. The GEV annual maxima model based on data from 1992 to 2019 resulted in 5.43 m as the 100-year return level for Vengurla and 5.82 m for Karwar. The 95th percentile value of H_s is 4.95 m at Vengurla and 5.10 m at Karwar, whereas the 90th percentile values are 4.78 m and 4.94 m respectively. The 100-year return period wave height values estimated with 20-year block data starting from 1992 to 2000, ranged from 4.91 to 5.63 at Vengurla and 5.73 to 6.48 m at Karwar (Table 5). At Vengurla, the 1992-2011 data block resulted in 5.63 m, while at Karwar, 1996-2015 data block resulted in 6.48 m. The higher 100-year return value at Karwar compared to Vengurla is due to the highest H_s of 5.19 m occurred on 29 May 2006. The lowest 100-year return value resulted for data from 1999-2018 at Vengurla (4.91 m) and 2000-2019 at Karwar (5.73 m). The maximum H_s of 5.1 m measured during 2015-2017 by the buoy is less than the estimated 100-year extremes for H_s of the study area.

The long-term trend of wave climate in the different parts of major oceans is studied (Young et al., 2011). Studies of trends in mean values of wave height over the last 30-40 years have shown small increases in mean significant wave height and these trends varied regionally with the largest increases in the Southern Hemisphere (Takbash and Young, 2019). The present study shows that from 1992 to 2019, the annual mean H_s shows a weak decreasing trend (0.093 to 0.14 cm/year), whereas H_{max} shows a slightly higher decreasing trend (0.33 and 0.27 cm/year) at the locations studied (Fig. 16). Sanil Kumar and Anoop (2015) observed that from 1979 to 2012, the average trend of annual mean H_s for all the locations in the western shelf seas is 0.06 cm/year. From 1979 to 2016, Nassef and Kumar (2017) observed a weak increasing trend (1.1 cm/year) in annual maximum H_s of the central west coast of India. Earlier many studies pointed out the difference in trend obtained by combining years before and after 1992 due to assimilation of altimeter wave heights into the reanalysis products starting in 1992 (Aarnes et al., 2014). If the data for 1979 to 2019 is considered, the trend in annual mean H_s in the present study is similar to the values (0.12 cm/year at Vengurla and 0.13 cm/year) reported earlier.

The trend in seasonal average significant wave height and maximum wave height during 1992 to 2019 is presented in Table 6. An increasing trend is observed during the southwest monsoon at both locations for significant wave height and maximum wave height. The trend value is similar for significant wave height (0.19 and 0.18 cm/year), whereas a significant difference in trend value is observed for maximum wave height during the southwest monsoon. While during the pre-monsoon and northeast monsoon periods decreasing trend is observed in both significant wave height and maximum wave height at both locations (Table 6).

4. Conclusions

This paper discussed the variations in wave spectral parameters within ~125 km along the eastern Arabian Sea. In the non-monsoon, the spectral characteristics are complicated by bi-directional conditions and two main frequency peaks could be recognized: one related to waves with T_p between 4 and 6 s and another related to waves with T_p between 12 and 16 s. Directional wave spectra indicate that the waves come predominantly from west/southwest, with an annual mean significant wave height of 1 m. Apart from the locally generated wind-sea, waves arriving at the central west coast of India can have three main generation sources. More energetic are those forced by southwest monsoon winds, followed by waves formed by northwest winds. Furthermore, there are the southern long-period swells. The characterization of the measured spectra shows a predominance of multi-modal cases (56 to 60%) due to the presence of significant wind-seas and swells and the unimodal spectra are relatively less. Spectral energy at the secondary spectral peak is ~38% of energy at the principal peak. The first mode of PC shows large variability ~90 % both at Vengurla and Karwar, which is due to the southwest monsoon and tropical cyclones Ashobaa (2015) and Ockhi (2017) in the Arabian Sea. The tropical cyclones (Ashobaa and Ockhi) caused large variations in wave parameters. Even though the study locations are within 125 km in the coastal waters having the same water depth, there is a large variation in wave height during some metrological events and caused variations in 100-year return period values of H_s . In addition, a large variation is observed in the 100-year return period value when different data blocks are used. The long-term trends observed in wave heights are relatively small. Even though the wave heights are reasonably well produced in the reanalysis datasets, the wave direction in the coastal regions where the co-existence of swells and wind-seas are in similar magnitudes, are poorly represented. The findings of the study based on measured buoy data presented here are to be confirmed with long-term measured data.

Acknowledgments

The authors acknowledge the high-performance computing resources made available at CSIR-NIO for conducting the research reported in this paper. Financial support is given by the Council of Scientific & Industrial Research, New Delhi, for wave measurements at Vengurla. The wave measurements at Karwar were part of the project funded by the Earth System Science Organization, Ministry of Earth Sciences, New Delhi. Dr. T. M. Balakrishnan Nair, Head OSISG, INCOIS, Hyderabad and Mr. Arun Nherakkol, scientist, INCOIS and Mr. Jai Singh, senior technical officer, CSIR-NIO, provided help during the data collection. ERA5 data used in this study are downloaded from the ECMWF data server: <http://data.ecmwf.int/data>. The authors thank both the reviewers for the comments and suggestions, which improved the scientific content of the paper. This paper is NIO contribution number ----.

References

- Aarnes, O.J., Abdalla, S., Bidlot, J., Breivik, Ø., 2014. Marine wind and wave height trends at different ERA-Interim forecast ranges. *Journal of Climate*, 28, 819-837, doi: 10.1175/JCLI-D-14-004701
- Aboobacker, V.M., Rashmi, R., Vethamony, P., Menon, H. B., 2011a. On the dominance of pre-existing swells over wind seas along the west coast of India, *Cont. Shelf Res.*, 31(16), 1701-1712, 2011. <https://doi.org/10.1016/j.csr.2011.07.010>
- Aboobacker, V.M., Vethamony, P. and Rashmi, R., 2011b. “Shamal” swells in the Arabian Sea and their influence along the west coast of India. *Geophys. Res. Lett.* 38(3), L03608. <https://doi.org/10.1029/2010GL045736>
- Alves, J.H.G.M., 2006. Numerical modeling of ocean swell contributions to the global wind-wave climate. *Ocean Model* 11:98–122. <https://doi.org/10.1016/j.ocemod.2004.11.007>
- Amante, C., Eakins, B., 2008. ETOPO1 1 Arc-Minute Global Relief Model: Procedures, Data Sources and Analysis (DOC/NOAA/NESDIS/NGDC).
- Amrutha, M.M., Sanil Kumar, V., George, J., 2017. Observations of long-period waves in the nearshore waters of central west coast of India during the fall inter-monsoon period. *Ocean Eng* 131:244–262. <https://doi.org/10.1016/j.oceaneng.2017.01.014>
- Amrutha, M.M., Sanil Kumar, V, Jai Singh, 2016. Changes in nearshore waves during the active sea/land breeze period off Vengurla, central west coast of India, *Annales Geophysicae*, 34, 215-226, doi:10.5194/angeo-34-215-2016
- Amrutha, M.M., Sanil Kumar, V., Sandhya, K.G., Nair, T.M.B., Rathod, J.L., 2016. Wave hindcast studies using SWAN nested in WAVEWATCH III - comparison with measured nearshore buoy data off Karwar, eastern Arabian Sea, *Ocean Engineering*, 119C, 114-124. [10.1016/j.oceaneng.2016.04.032](https://doi.org/10.1016/j.oceaneng.2016.04.032)
- Anjali Nair, M., Sanil Kumar, V., 2016. Spectral wave climatology off Ratnagiri - northeast Arabian Sea, *Natural Hazards*, 82, 1565-1588.
- Anjali Nair, M., Sanil Kumar, V., 2017. Wave spectral shapes in the coastal waters based on measured data off Karwar on the west coast of India, *Ocean Science*, 13, 365–378, doi:10.5194/os-13-365-2017
- Anoop, T.R. Sanil Kumar, V., Johnson Glejin, 2014, A study on reflection pattern of swells from the shoreline of peninsular India, *Natural Hazards*, 74, 1863-1879 DOI:10.1007/s11069-014-1282-5
- Anoop, T.R., Sanil Kumar, V., Shanas, P.R., Johnson, G. 2015. Surface wave climatology and its variability in the North Indian Ocean based on ERA-Interim reanalysis. *J Atmos Ocean Technol* 32(7):1372–1385. <https://doi.org/10.1175/JTECH-D-14-00212.1>
- Anoop, T.R., Shanas, P.R., Aboobacker, V.M., Sanil Kumar, V., Nair, L.S., Prasad, R., Reji, S., 2020. On the generation and propagation of Makran swells in the Arabian Sea. *Int. J. climatology* 40 (1): 585-593. <https://doi.org/10.1002/joc.6192>

- Ardhuin, F., O'Reilly, W.C., Herbers, T.H.C., Jessen, P.F., 2003. Swell transformation across the continental shelf. Part I: Attenuation and Directional Broadening, *Journal of Physical Oceanography*, 33(9), 1921–1939. [https://doi.org/10.1175/1520-0485\(2003\)033<1921:STATCS>2.0.CO;2](https://doi.org/10.1175/1520-0485(2003)033<1921:STATCS>2.0.CO;2)
- Banner, M., Young, I.R., 1994. Modeling spectral dissipation in the evolution of wind waves. *J. Phys. Oceanogr.*, 24, 1550–1561. [https://doi.org/10.1175/1520-0485\(1994\)024<1550:MSDITE>2.0.CO;2](https://doi.org/10.1175/1520-0485(1994)024<1550:MSDITE>2.0.CO;2)
- Chandramohan, P., Sanil Kumar, V., Nayak, B.U, 1991. Wave statistics around the Indian coast based on ship observed data. *Indian Journal of Marine Sciences*, 20 (2), 87-92.
- Chawla, A., Tolman, H.L., Gerald, V., Spindler, D., Spindler, T., Alves, J.G., Cao, D., Hanson, J.L, Devaliere, E., 2013. A Multigrid Wave Forecasting Model: A New Paradigm in Operational Wave Forecasting. *Weather Forecasting*, 28, 1057-1078, <https://doi.org/10.1175/WAF-D-12-00007.1>
- Crosby, S.C., O'Reilly, W.C., Guza, R., 2016. Modeling long-period swell in southern California: Practical boundary conditions from buoys observations and global wave model predictions, *J. Atmos. Oceanic Technol.*, 33, 1673–1690, doi:10.1175/JTECH-D-16-0038,1.
- Cuchiara, D.C., Fernandes, E.H., Strauch, J.C., Winterwerp, J.C., Calliari, L.J., 2009. Determination of the wave climate for the southern Brazilian shelf, *Continental Shelf Research* 29: 545–555. <https://doi.org/10.1016/j.csr.2008.09.025>
- Datawell, 2009. *Datawell Waverider Reference Manual*. Datawell BV Oceanographic Instruments: Haarlem, The Netherlands, p. 123.
- Donelan, M., Hamilton, H., and Hui, W.H., 1985. Directional spectra of wind-generated waves, *Philosophical Transactions of the Royal Society of London A: Mathematical, Physical and Engineering Sciences.*, 315(1534), 509-562.
- Elgar, S., Herbers, T., Guza, R., 1994. Reflection of ocean surface gravity waves from a natural beach. *J Phys Oceanogr* 24(7):1503–1511. [https://doi.org/10.1175/1520-0485\(1994\)024<1503:ROOSGW>2.0.CO;2](https://doi.org/10.1175/1520-0485(1994)024<1503:ROOSGW>2.0.CO;2)
- Findlater, J., 1969. A major low-level air current near the Indian Ocean during the northern summer. *Quarterly Journal of the Royal Meteorological Society*, 95(404), 362–380. <https://doi.org/10.1002/qj.49709540409>.
- Forristall, G., Ewans, K., 1998. Worldwide measurements of directional wave spreading. *J. Atmos. Oceanic Technol.*, 15, 440–469. [https://doi.org/10.1175/1520-0426\(1998\)015<0440:WMODWS>2.0.CO;2](https://doi.org/10.1175/1520-0426(1998)015<0440:WMODWS>2.0.CO;2)
- George, J., Sanil Kumar, V., Gowthaman, R., Singh, J., 2020. Nearshore wave characteristics and longshore sediment transport along a micro-tidal wave-dominated coast having comparable wind-sea and swell energy, *Journal of Marine Science and Engineering* 8, 55; <https://doi.org/10.3390/jmse8010055>
- Glejin, J., Sanil Kumar, V., Nair, B., Singh, J., 2013. Influence of winds on temporally varying short and long period gravity waves in the near shore regions of the eastern Arabian Sea. *Ocean Science* 9(2):343-353. doi:10.5194/os-9-343-2013

- Goda, Y., 1992. Uncertainty of design parameters from viewpoint of extreme statistics, *J Offshore Mech Arct.*, 114(2), 76-82, 1992.
- Harvey, N., Woodroffe, C. D., 2008. Australian approaches to coastal vulnerability assessment. *Sustainability Science* 3(1), 67–87. doi:10.1007/S11625-008-0041-5.
- Hasselmann, K., Barnett, T.P., Bouws, F., Carlson, H., Cartwright, D.E., Enke, K., Ewing J.A., Gienapp, H., Hasselmann, D.E., Krusemann, P., Meerburg, A., Muller, P., Olbers, D.J., Richter, K., Sell, W., and Walden, H., 1973. Measurements of wind-wave growth and swell decay during the Joint North Sea Wave Project (JONSWAP), *Deutsches Hydrographisches Institut.*, A8 (12), 95.
- Hersbach, H., Bell, B., Berrisford, P, et al., 2020. The ERA5 global reanalysis. *Q J R Meteorol Soc.* 146, 1999– 2049. <https://doi.org/10.1002/qj.3803>
- IMD, 2016, Report on cyclonic disturbances over north Indian Ocean during 2015: A Report. RSMC New Delhi, India Meteorological Department. No. ESSO/IMD/RSMC-Tropical Cyclones Report No. 01 (2016)/14, 338p, Retrieved December 15, 2018. <http://www.rsmcnewdelhi.imd.gov.in/images/pdf/publications/annual-rsmc-report/RSMC-2015.pdf>.
- IMD, 2017, Very Severe Cyclonic Storm "Ockhi" over Bay of Bengal (29 November 2017-06 December 2017): A Report. RSMC New Delhi, India Meteorological Department. Retrieved December 15, 2018.
- Kotal, S.D, Bhattacharya, S.K., Sharma, A., Bhowmik, S.K.R., 2016. NWP Report on cyclonic storms over the north Indian Ocean during 2015, India Meteorological Department (Numerical Weather Prediction Division) Earth System Science Organization (ESSO) Ministry of Earth Sciences (MoES)
- Kuik, A.J., Vledder, G., Holthuijsen, L.H., 1988. A method for the routine analysis of pitch and roll buoy wave data, *Journal of Physical Oceanography*, 18, 1020-1034. [https://doi.org/10.1175/1520-0485\(1988\)018<1020:AMFTRA>2.0.CO;2](https://doi.org/10.1175/1520-0485(1988)018<1020:AMFTRA>2.0.CO;2)
- Kumar, V.S., Deo, M.C., Anand, N.M., Chandramohan, P., 1999. Estimation of wave directional spreading in shallow water, *Ocean Engineering*, 26(2), 83-98. [https://doi.org/10.1016/S0029-8018\(97\)10014-2](https://doi.org/10.1016/S0029-8018(97)10014-2)
- Kumar, V.S., Anand, N.M., Ashok Kumar, K., Mandal, S., 2003. Multipeakedness and groupiness of shallow water waves along Indian coast, *Journal of Coastal Research*, 19(4), 1052-1065. <https://doi.org/10.1007/s12040-012-0160-3>
- Kumar, V.S., Anand, N.M., 2004. Variations in wave direction estimated using first and second order Fourier coefficients, *Ocean Engineering*, 31, 2105–2119. <https://doi.org/10.1016/j.oceaneng.2004.06.003>
- Kumar, V.S., George, J., Dora, U., Naseef, M., 2019. Surface wave dynamics off Mumbai coast, north-eastern Arabian Sea, *Ocean Dynamics*, 69, 29-42, <https://doi.org/10.1007/s10236-018-1230-0>
- Kumar, V.S., Pathak, K.C., Pednekar, P., Raju, N.S.N., Gowthaman, R., 2006. Coastal processes along the Indian coastline. *Current Science*, 91(4), 530-536

- Kumar, V.S., Shanas, P.R., Dubhashi, K.K., 2014. Shallow water wave spectral characteristics along the eastern Arabian Sea, *Natural Hazards* 70, 377–394, doi: 10.1007/s11069-013-0815-7
- Kumar, V.S., Sajiv Philip, C., Nair, T.N.B., 2010, Waves in shallow water off west coast of India during the onset of summer monsoon, *Annales Geophysicae*, 28, 817–824. doi:10.5194/angeo-28-817-2010
- Masselink, G., Pattiaratchi, C.B., 2001. Characteristics of the Sea Breeze System in Perth, Western Australia, and Its Effect on the Nearshore Wave Climate. *Journal of Coastal Research*, 17(1), 173-187
- Naseef, T.M, Kumar, V.S, 2017. Variations in return value estimate of ocean surface waves – a study based on measured buoy data and ERA-Interim reanalysis data, *Natural Hazards Earth System Sciences*, 17, 1763–1778, doi: 10.5194/nhess-17-1763-2017
- Naseef, T.M., Kumar, V.S., 2020. Climatology and trends of the Indian Ocean surface waves based on 39-year long ERA5 reanalysis data, *International Journal of Climatology*, 40, 979-1006, doi.org/10.1002/joc.6251
- Orimoloye, S., Karunarathna, H., Reeve, D.E., 2019. Effects of Swell on Wave Height Distribution of Energy-Conserved Bimodal Seas. *J. Mar. Sci. Eng.* 2019, 7, 79. <https://doi.org/10.3390/jmse7030079>
- Portilla, J., Ocampo-Torres, F.J., Monbaliu, J., 2009. Spectral Partitioning and Identification of Wind Sea and Swell. *Journal of Atmospheric and Oceanic Technology*, 26, 117–122.
- Portilla, J., Salazar, A., Cavaleri, L., 2016. Climate patterns derived from ocean wave spectra. *Geophysical Research Letters*, 43, 11,736–11,743. <https://doi.org/10.1002/2016GL071419>
- Preisendorfer, R. W., Mobley, C. D., 1988. *Principal component analysis in meteorology and oceanography* (Vol. 425). Amsterdam: Elsevier
- Rueda, A., Hegermiller, C.A., Antolinez, J. A. A, Camus, P., Vitousek, S., Ruggiero, P., Barnard, P.L., Erikson, L.H., Tomas, A., Mendez, F.J., 2017. Multiscale climate emulator of multimodal wave spectra: MUSCLEspectra, *J. Geophys. Res. Oceans*, 122, 1400–1415, doi:10.1002/2016JC011957
- Sanil Kumar, V., Anoop, T.R., 2015. Spatial and temporal variations of wave height in shelf seas around India, *Nat. Hazards*, 78, 1693-1706. doi: 10.1007/s11069-015-1796-5
- Semedo, A., Suselj, K., Rutgersson, A., Sterl, A., 2011. A global view on the wind sea and swell climate and variability from ERA-40, *J. Clim.*, 24, 1461–1479. <https://doi.org/10.1175/2010JCLI3718.1>
- Soares, C.G., 1991. On the occurrence of double peaked wave spectra. *Ocean Eng.* 18(1/2), 167-171. [https://doi.org/10.1016/0029-8018\(84\)90019-2](https://doi.org/10.1016/0029-8018(84)90019-2)
- Sverdrup, H. U., Munk, W.H., 1947. *Wind sea and swell: theory of relations for forecasting*, US Hydrographic Office, Washington, D.C, 601
- Takbash, A., Young, I.R., 2019. Global ocean extreme wave heights from spatial ensemble data. *Journal of Climate* 32, no. 20, 6823-6836

Thornton, E. B., Guza, R. T., 1986. Surf zone longshore currents and random waves: Field data and models. *Journal of Physical Oceanography*, 16(7), 1165–1178. DOI: 10.1175/1520-0485(1986)016<1165:szlcar>2.0.co;2

Tolkova, E., 2010. EOF analysis of a time series with application to tsunami detection. *Dynamics of Atmospheres and Oceans*, 50(1), pp.35-54

Tolman, H.L., 1991. A third-generation model for wind waves on slowly varying, unsteady and inhomogeneous depths and currents. *J. Phys. Oceanogr.* 21, 782–797

Young, I. R., Zieger, S., Babanin, A. V., 2011. Global trends in wind speed and wave height. *Science* 332(6028), 451-455. doi:10.1126/SCIENCE.1197219

Young, I.R., Verhagen, L.A., Banner, M. L., 1995. A note on the bimodal directional spreading of fetch-limited wind waves, *J. Geophys. Res.*, 100 (C1), 773–778. <https://doi.org/10.1029/94JC02218>

Table 1. List of tropical cyclones formed in Arabian Sea during 2015 to 2017

Year	Tropical Cyclone	Area & Time
2015	Ashobaa	East-Central Arabian sea 7-12 June
	Chapala	South-East Arabian Sea 28 Oct - 4 Nov
	Megh	East-central Arabian Sea 5-10 Nov
2017	Ockhi	Originate South-West Bay of Bengal and Migrated to North-West Arabian Sea 28 Nov - 6 Dec

Table 2. Average wave parameters during different seasons and annually at Karwar and Vengurla in different years

Location	Year	Period	Significant wave height (m)	Mean wave period (s)	Peak wave period (s)	Maximum wave height (m)	Swell (%)	Spectral energy density at spectral peak (m ² /Hz)
Karwar	2015	Feb-May	0.73	4.82	12.16	1.10	48	0.66
		Jun-Sep	1.83	6.10	10.98	2.82	66	5.53
		Oct-Jan	0.67	4.98	12.63	1.01	50	0.70
		Jan-Dec	1.11	5.35	11.90	1.71	55	2.48
	2016	Feb-May	0.91	4.77	11.07	1.38	40	1.13
		Jun-Sep	2.06	6.40	10.53	3.19	72	6.71
		Oct-Jan	0.61	4.92	12.88	0.93	50	0.60
		Jan-Dec	1.16	5.32	11.54	1.78	53	2.66
	2017	Feb-May	0.79	4.92	11.31	1.20	44	0.83
		Jun-Sep	1.97	6.49	10.50	3.05	73	6.15
		Oct-Jan	0.67	4.78	11.62	1.02	45	0.61
		Jan-Dec	1.15	5.40	11.14	1.76	54	2.54
Vengurla	2015	Feb-May	0.63	4.50	12.05	0.95	43	0.46
		Jun-Sep	1.62	6.00	10.24	2.50	68	4.29
		Oct-Jan	0.54	5.01	12.60	0.83	51	0.40
		Jan-Dec	0.93	5.17	11.63	1.43	54	1.72
	2016	Feb-May	0.76	4.61	11.74	1.14	43	0.81
		Jun-Sep	1.95	6.48	10.60	2.98	75	6.50
		Oct-Jan	0.48	4.93	12.88	0.72	52	0.35
		Jan-Dec	1.04	5.31	11.76	1.58	56	2.46
	2017	Feb-May	0.66	4.64	11.54	1.00	44	0.57
		Jun-Sep	1.76	6.48	10.45	2.72	75	5.55
		Oct-Jan	0.53	4.83	12.13	0.80	48	0.44
		Jan-Dec	0.98	5.32	11.38	1.51	56	2.19

Table 3. Percentage of single-peaked and multi-peaked wave spectra in different months of 2017 along with classification as wind-sea, swell or mixed based on spectral peak period

Month	Single-peak (%)				Multi-peak (%)			
	Total	Wind-sea ($T_p < 6$)	Swell ($T_p > 8$)	Mixed ($6 < T_p < 8$)	Total	Wind-sea dominated ($T_p < 6$)	Swell dominated ($T_p > 8$)	Mixed ($6 < T_p < 8$)
Karwar								
January	21.64	0.60	20.50	0.54	78.36	17.54	49.87	10.95
February	21.88	0.37	21.21	0.30	78.13	29.91	34.82	13.39
March	5.94	0.81	3.04	2.09	94.06	31.71	51.21	11.13
April	19.10	0.07	19.03	0.00	80.90	14.03	61.04	5.83
May	56.79	0.00	56.72	0.07	43.21	1.14	38.44	3.63
June	75.42	0.00	75.35	0.07	24.58	0.00	24.17	0.42
July	74.46	0.00	74.46	0.00	25.54	0.00	25.54	0.00
August	59.74	0.00	59.21	0.54	40.26	0.00	32.33	7.93
September	31.74	0.00	31.60	0.14	68.26	1.53	56.88	9.86
October	27.76	0.00	27.55	0.20	72.24	5.51	56.72	10.01
November	39.33	0.28	38.41	0.64	60.67	9.64	42.59	8.43
December	39.10	0.21	38.47	0.42	60.90	19.20	34.34	7.36
Annual average	39.41	0.20	38.79	0.42	60.59	10.85	42.33	7.41
Vengurla								
January	31.38	0.20	30.78	0.40	68.62	9.01	55.44	4.17
February	27.38	0.22	27.01	0.15	72.62	24.40	40.70	7.51
March	10.43	0.20	9.89	0.34	89.57	18.03	66.08	5.45
April	15.63	0.14	15.35	0.14	84.38	18.40	62.15	3.82
May	56.52	0.00	56.25	0.27	43.48	0.40	37.84	5.24
June	83.75	0.00	83.75	0.00	16.25	0.00	16.11	0.14
July	80.85	0.00	80.85	0.00	19.15	0.00	19.15	0.00
August	66.20	0.00	65.73	0.47	33.80	0.07	25.81	7.93
September	38.96	0.21	37.29	1.46	61.04	1.53	52.50	7.01
October	25.07	0.00	25.07	0.00	74.93	4.37	62.63	7.93
November	42.11	0.00	41.70	0.42	57.89	5.98	46.91	5.00
December	45.27	0.13	45.06	0.07	54.73	16.05	31.03	7.66
Annual average	43.63	0.09	43.23	0.31	56.37	8.19	43.03	5.16

Table 4. Percentage of waves from different direction sectors at Karwar and Vengurla during different years

Location	Year	Swell (%)			Wind-sea (%)			
		Direction (deg)	February-May	June-September	October-January	February-May	June-September	October-January
Karwar	2015	0-168	3.61	1.79	3.38	5.34	3.00	9.51
		168-248	35.32	14.53	34.85	6.34	11.25	8.49
		248-276	3.47	37.46	3.13	8.18	14.11	3.86
		276-360	2.39	5.52	3.42	35.34	12.33	33.36
	2016	0-168	2.48	1.65	2.94	5.50	2.59	7.97
		168-248	27.10	17.69	40.21	4.53	8.77	7.30
		248-276	5.00	36.61	2.41	5.77	15.06	4.96
		276-360	2.43	5.10	1.73	47.18	12.53	32.49
	2017	0-168	2.31	1.57	2.55	4.55	2.00	8.06
		168-248	32.30	18.80	34.33	6.14	9.45	10.19
		248-276	4.66	41.21	3.56	18.52	19.95	10.37
		276-360	1.48	1.25	1.42	30.05	5.77	29.51
Vengurla	2015	0-168	3.14	0.93	3.98	3.56	1.57	5.21
		168-248	31.80	24.37	37.03	6.71	14.89	13.02
		248-276	2.78	26.19	3.28	9.73	14.62	5.64
		276-360	2.39	4.76	2.73	39.88	12.68	29.10
	2016	0-168	3.04	0.99	4.70	3.31	1.11	4.18
		168-248	27.36	20.40	39.24	5.48	12.48	9.02
		248-276	6.57	38.56	2.49	10.60	14.65	6.97
		276-360	2.72	4.06	2.02	40.92	7.76	31.37
	2017	0-168	3.40	0.68	3.51	3.27	1.06	3.67
		168-248	30.48	20.86	36.10	7.97	12.53	11.60
		248-276	4.14	38.72	2.56	12.74	13.92	7.07
		276-360	2.22	3.66	2.24	35.78	8.56	33.24

Table 5. 100-year return period wave height based on Generalised extreme value distribution with annual maximum data at Vengurla and Karwar estimated using ERA5 significant wave height with different data periods

Data block	100-year return period wave height (m)	
	Vengurla	Karwar
1992-2019	5.43	5.82
1992-2011	5.63	6.17
1993-2012	5.43	5.99
1994-2013	5.52	6.32
1995-2014	5.58	6.43
1996-2015	5.51	6.48
1997-2016	5.17	6.03
1998-2017	5.02	6.12
1999-2018	4.91	5.91
2000-2019	5.14	5.73

Table 6. Long-term trend in seasonal average significant wave height and maximum wave height

Parameter	Location	Trend in different seasons (cm/year)		
		Pre-monsoon (February-May)	Southwest monsoon (June-September)	Northeast monsoon (October-January)
Significant wave height	Vengurla	-0.30	0.19	-0.10
	Karwar	-0.35	0.18	-0.14
Maximum wave height	Vengurla	-0.84	0.02	-0.30
	Karwar	-0.67	0.31	-0.26

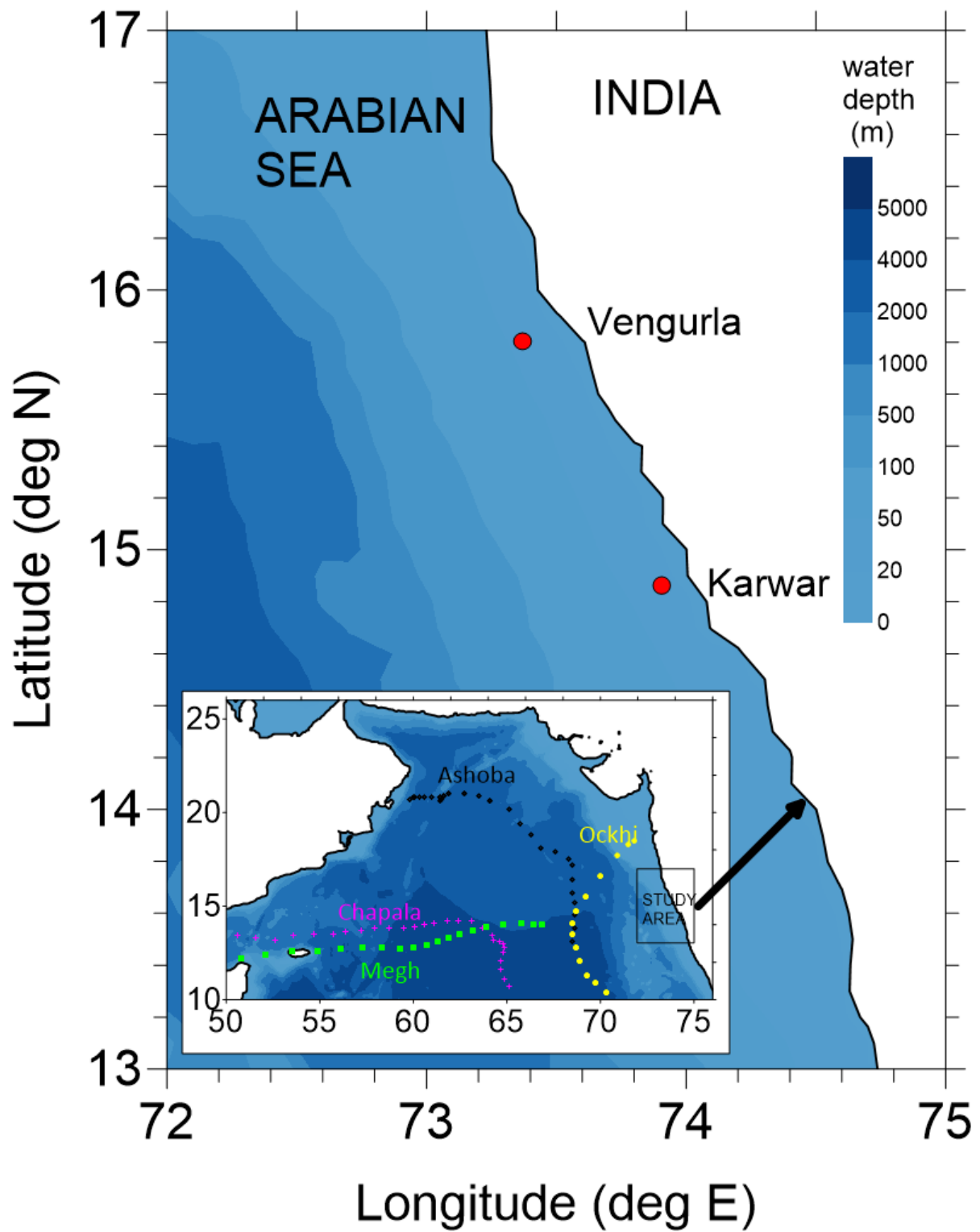


Figure 1. Location map showing the wave buoy positions in the eastern Arabian Sea. Tracks of all the tropical cyclones formed in Arabian Sea during 2015-2017 is also shown

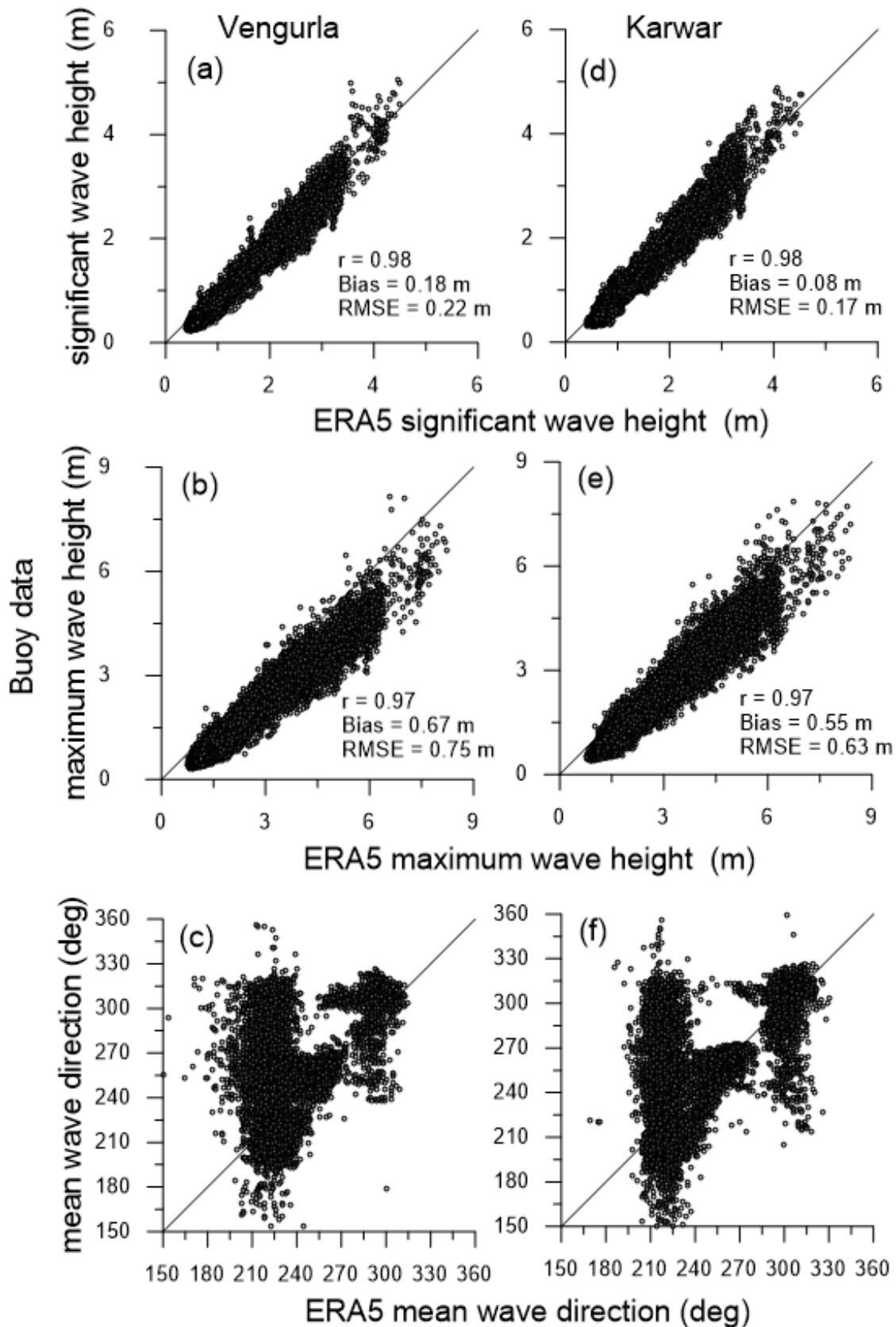


Figure 2. Scatter plots of ERA5 wave data with buoy data a) and d) significant wave height (H_s), b) and e) maximum wave height (H_{max}), c) and f) mean wave direction. The left panel is for Vengurla and the right panel is for Karwar

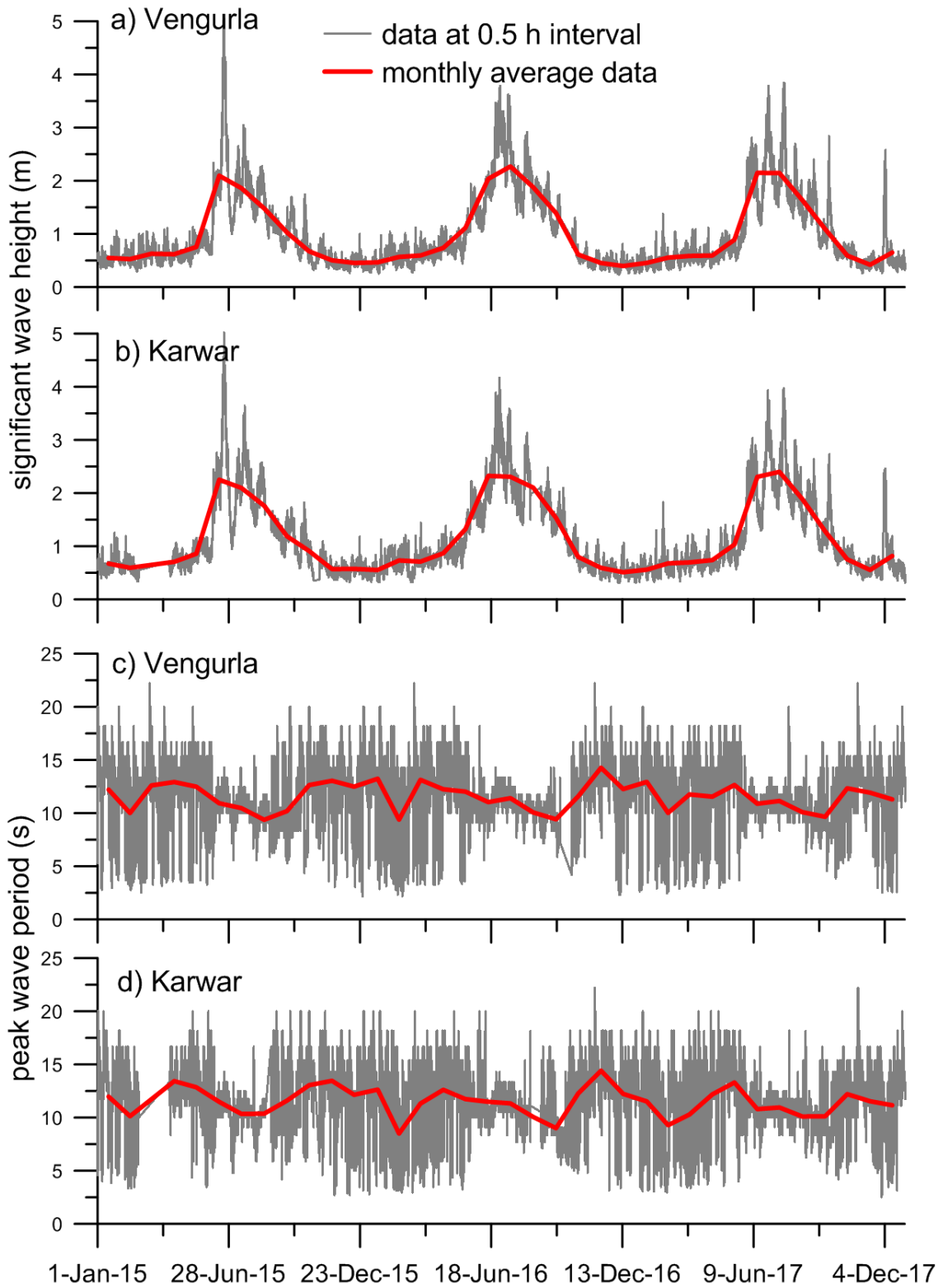


Figure 3. Time series plot of significant wave height and peak wave period at Vengurla and Karwar from 1 January 2015 to 31 December 2017. The thick solid line indicate the monthly average values

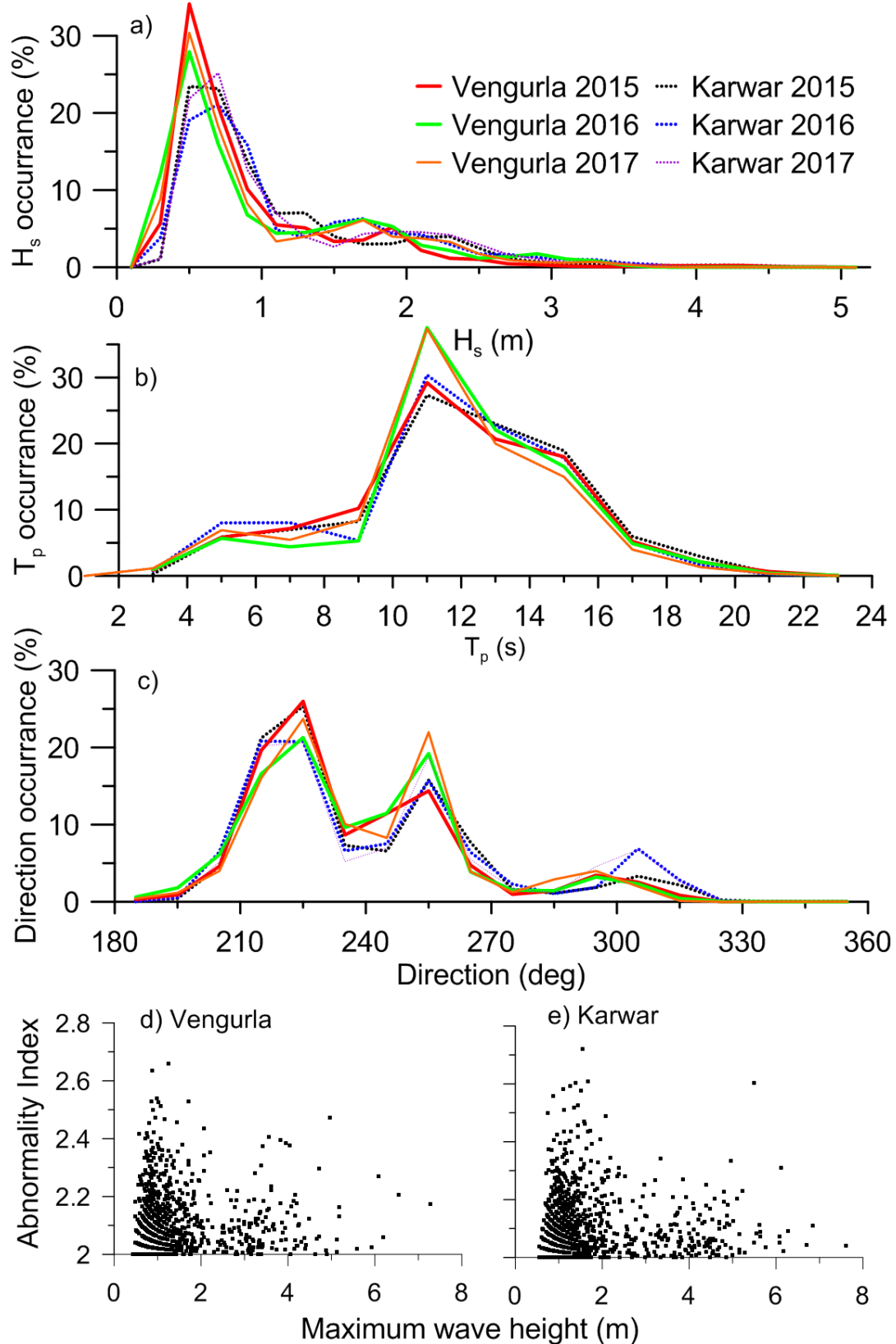


Figure 4. a) Statistical distribution of significant wave heights, b) peak wave period and c) mean wave direction at Vengurla and Karwar during 2015, 2016 and 2017, d) and e) plot of abnormality index with maximum wave height at Vengurla and Karwar

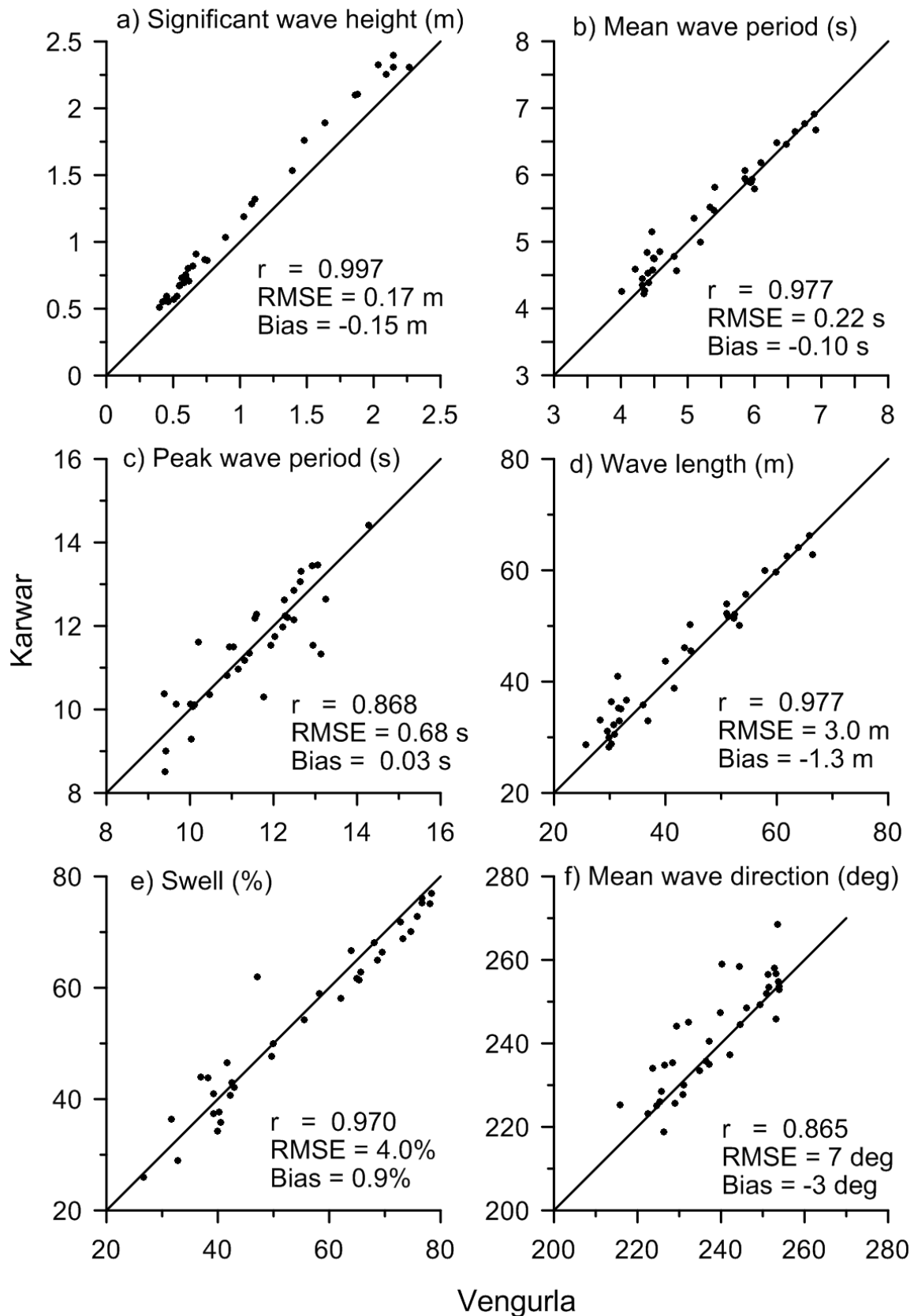


Figure 5. Comparison of monthly average wave parameters at Vengurla and Karwar a) significant wave height, b) mean wave period, c) peak wave period, d) wave length, e) swell (%) and f) mean wave direction

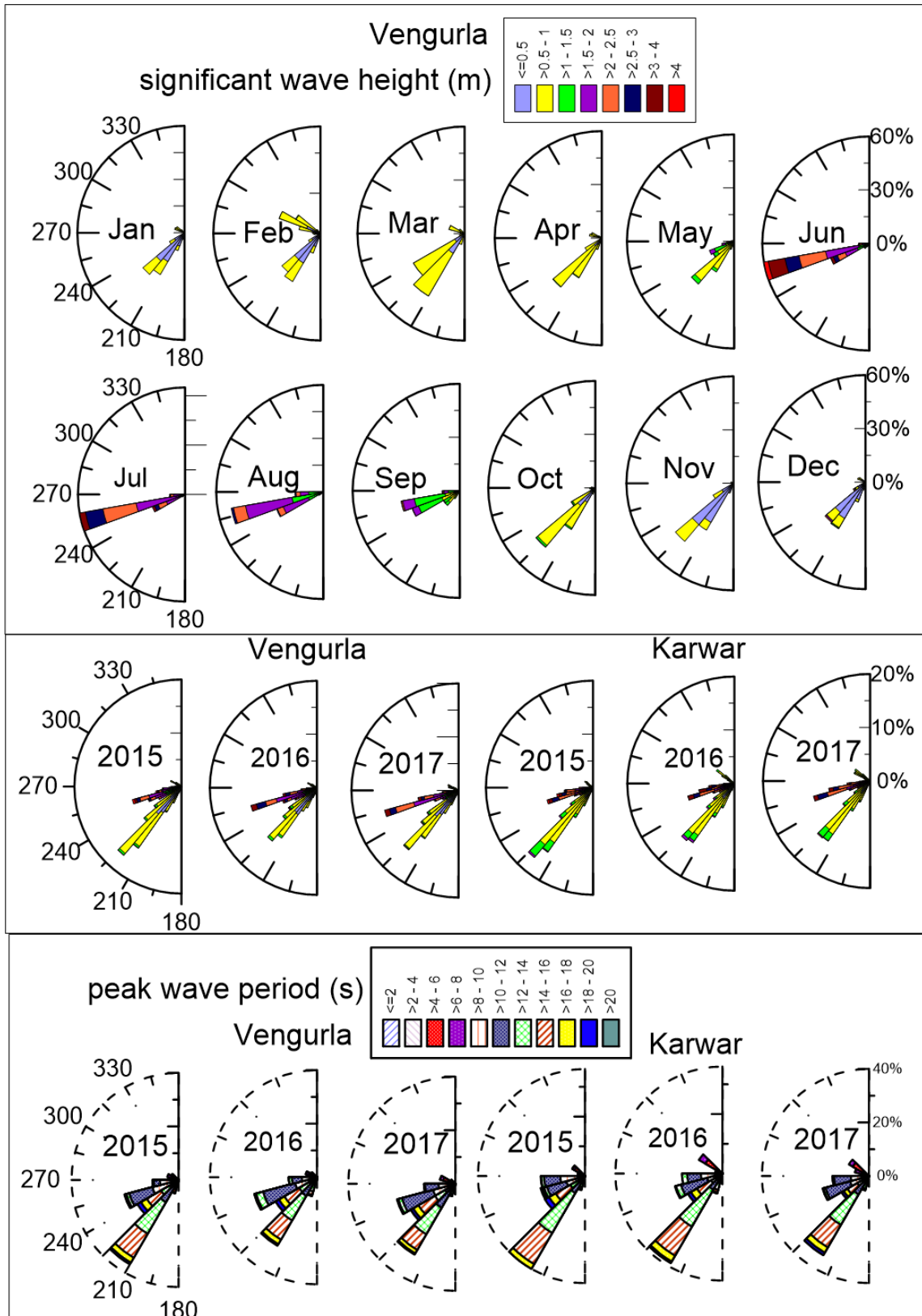


Figure 6. Top panel shows the monthly wave rose diagram of significant wave height at Vengurla in 2015. Middle panel is the annual wave height roses for Vengurla and Karwar in 2015, 2016 and 2017. Bottom panel is the wave rose diagram of peak wave period at Vengurla and Karwar in different years. The direction represents where the waves comes from

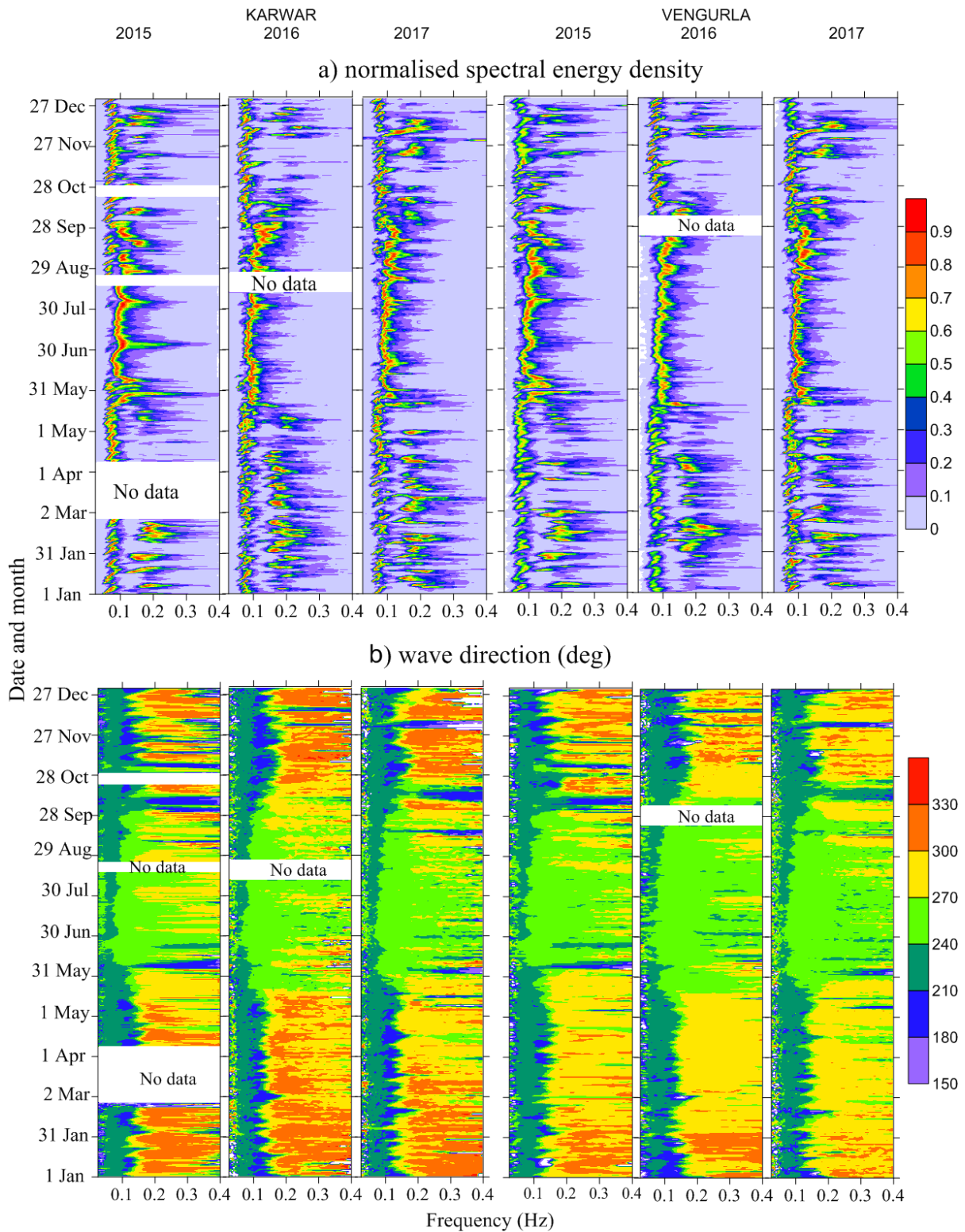


Figure 7. Contour plots of a) normalised spectral energy density of the sea surface height variance and b) mean wave direction. Normalized spectral density of the sea surface height variance is obtained by dividing the spectral density at each frequency by the maximum spectral density of the sea surface height variance of the respective wave spectrum

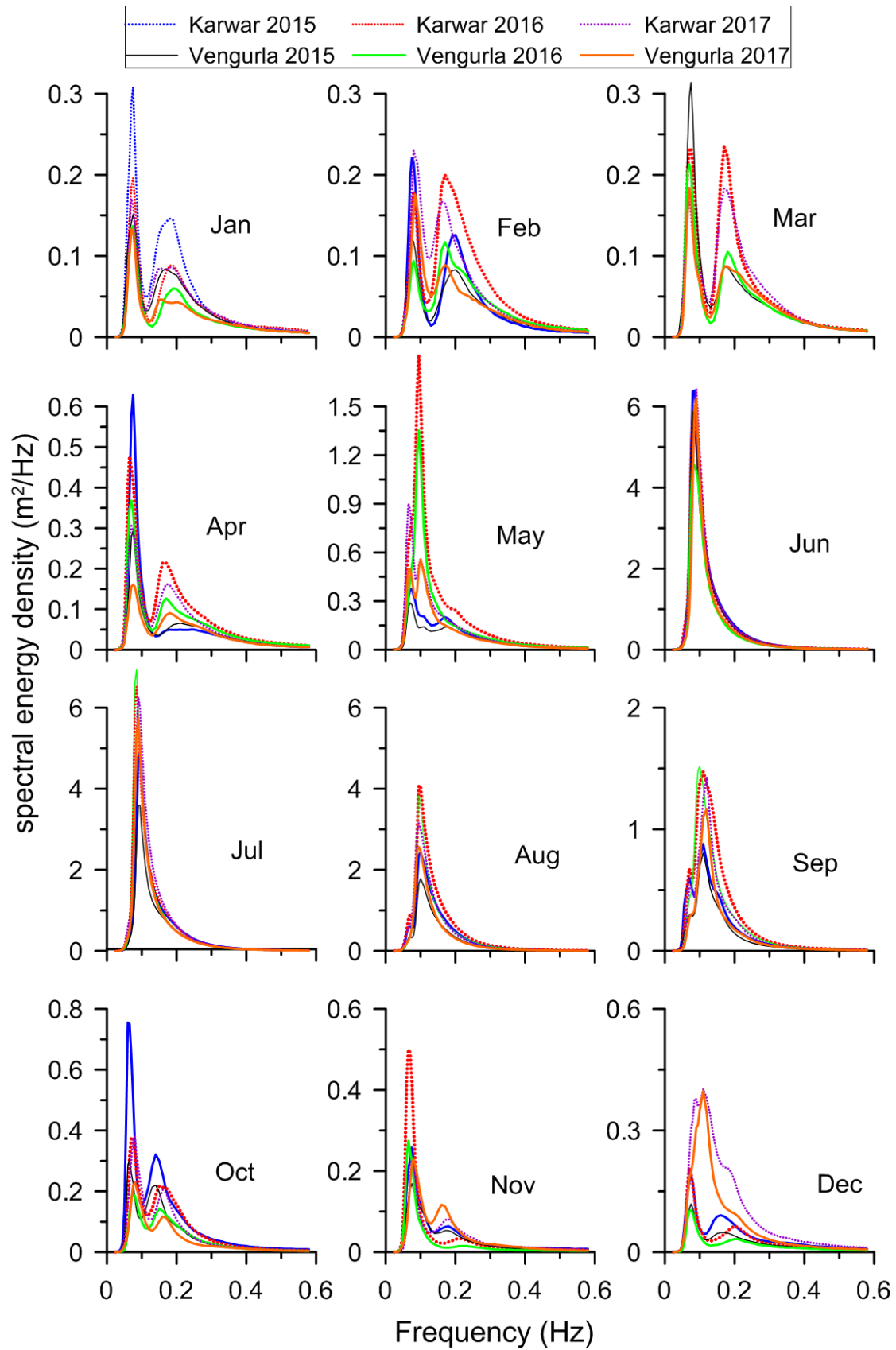


Figure 8. Monthly average wave spectra for Vengurla and Karwar during 2015, 2016 and 2017

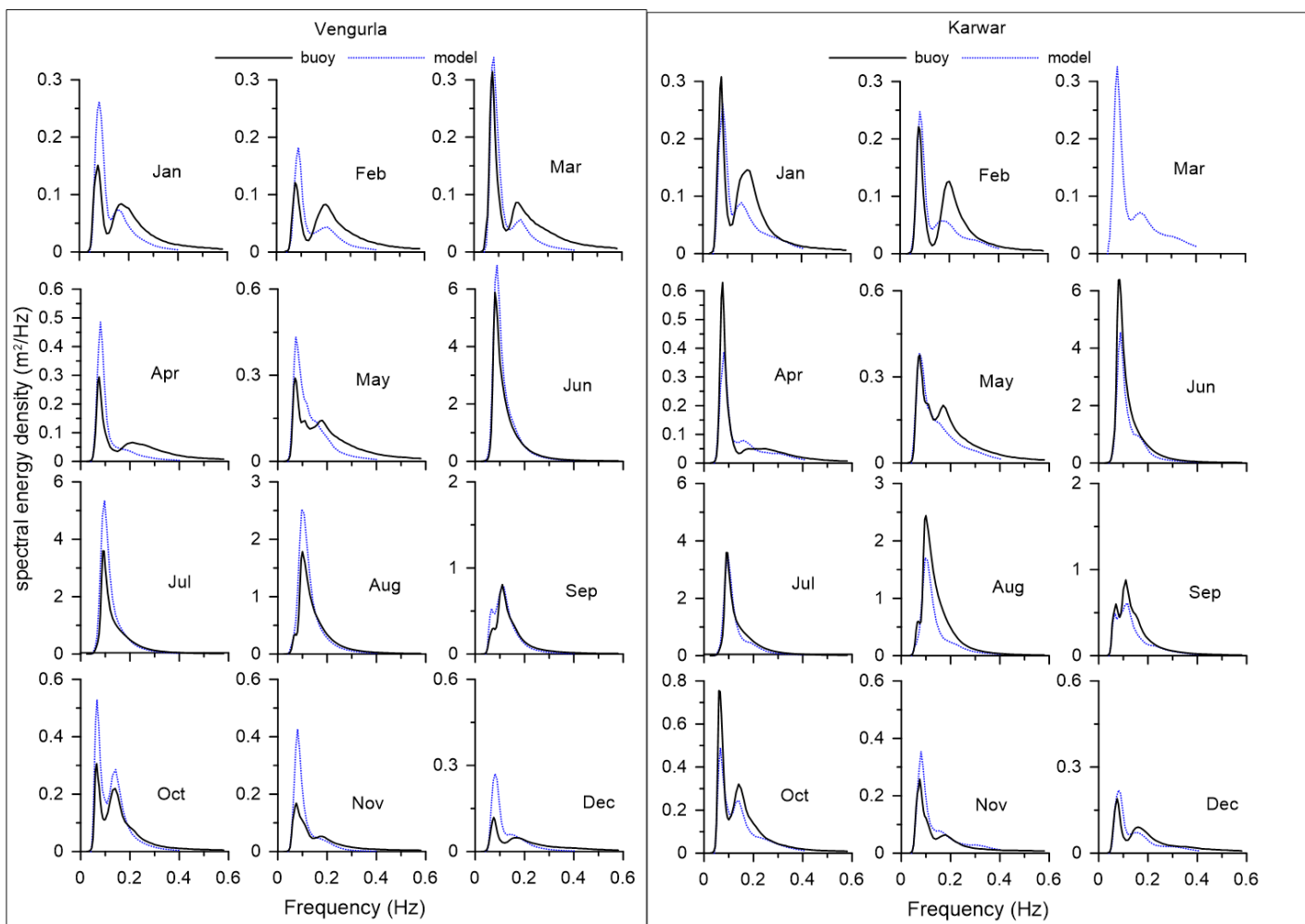


Figure 9. Comparison of monthly average wave spectra from numerical model and buoy data in 2015. Left panel is for Vengurla and right panel is for Karwar

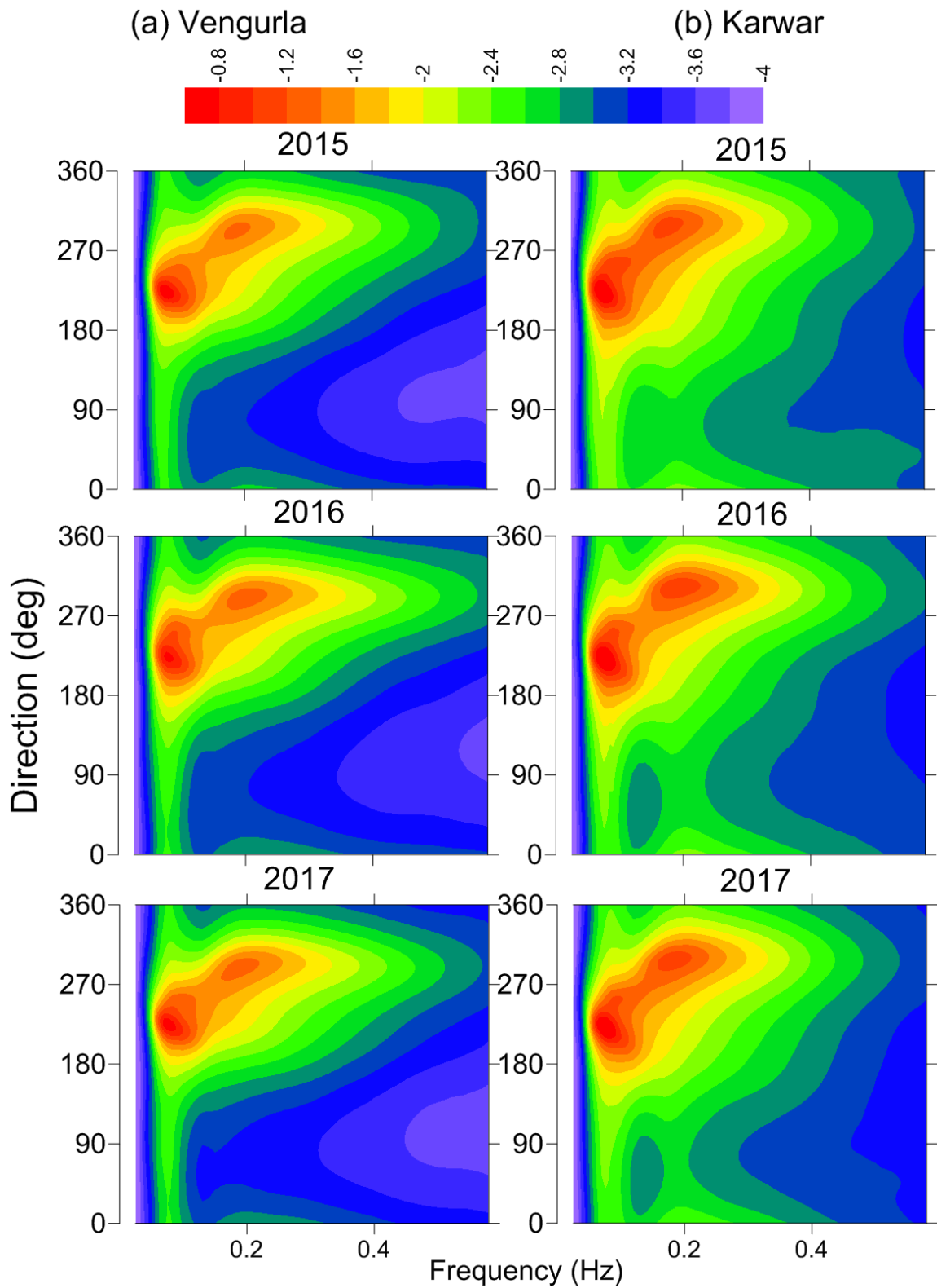


Figure 10. Annual average wave spectra in different years at Karwar and Vengurla. The color bar is for spectral energy ($\text{m}^2/\text{deg}/\text{Hz}$). The spectral energy is shown in logarithmic scale (base 10)

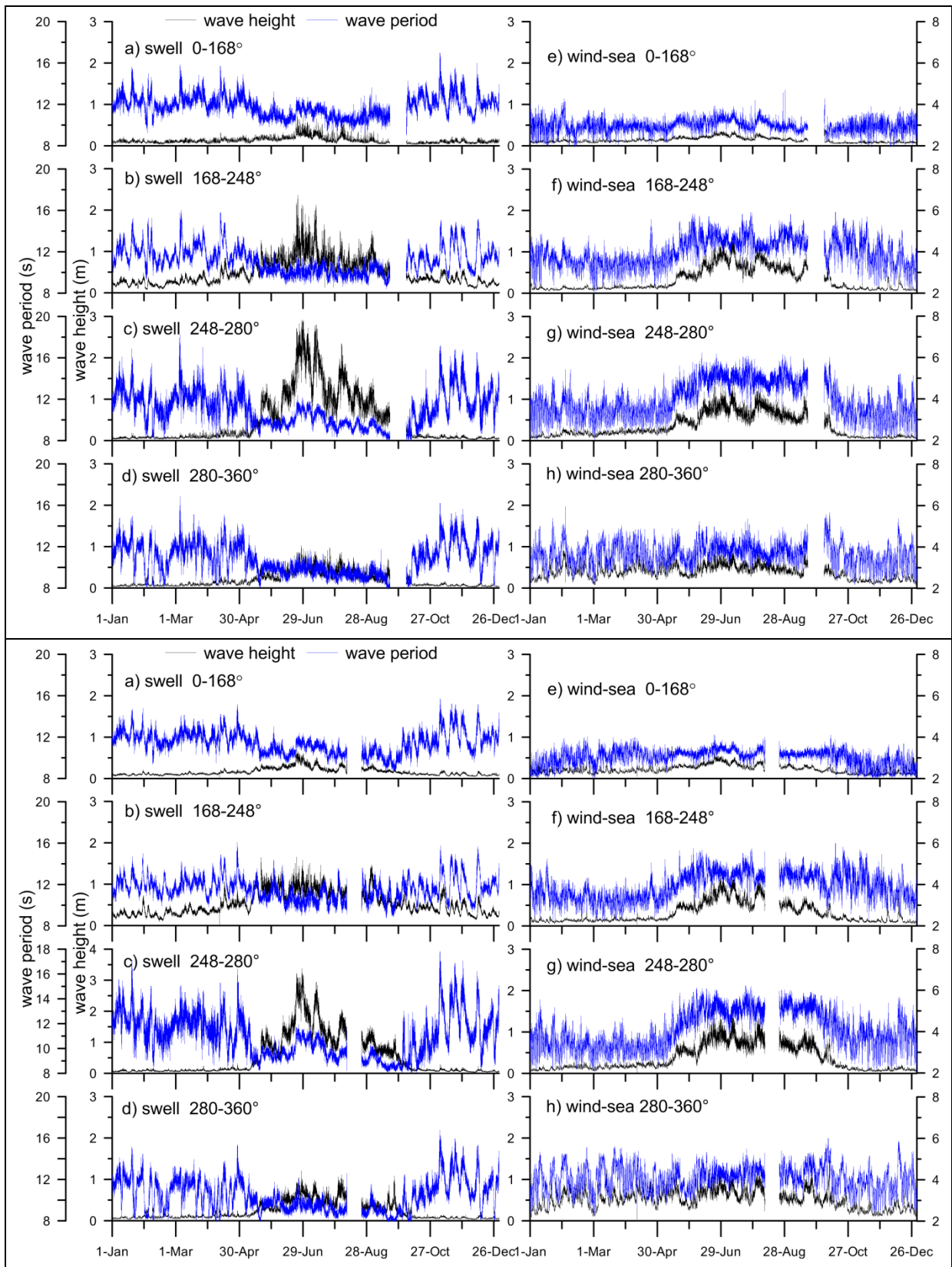


Figure 11. Time series plot of significant wave height and mean wave period of swell and wind-sea from different directions during 2016. Top panel is for Vengurla and bottom panel is for Karwar

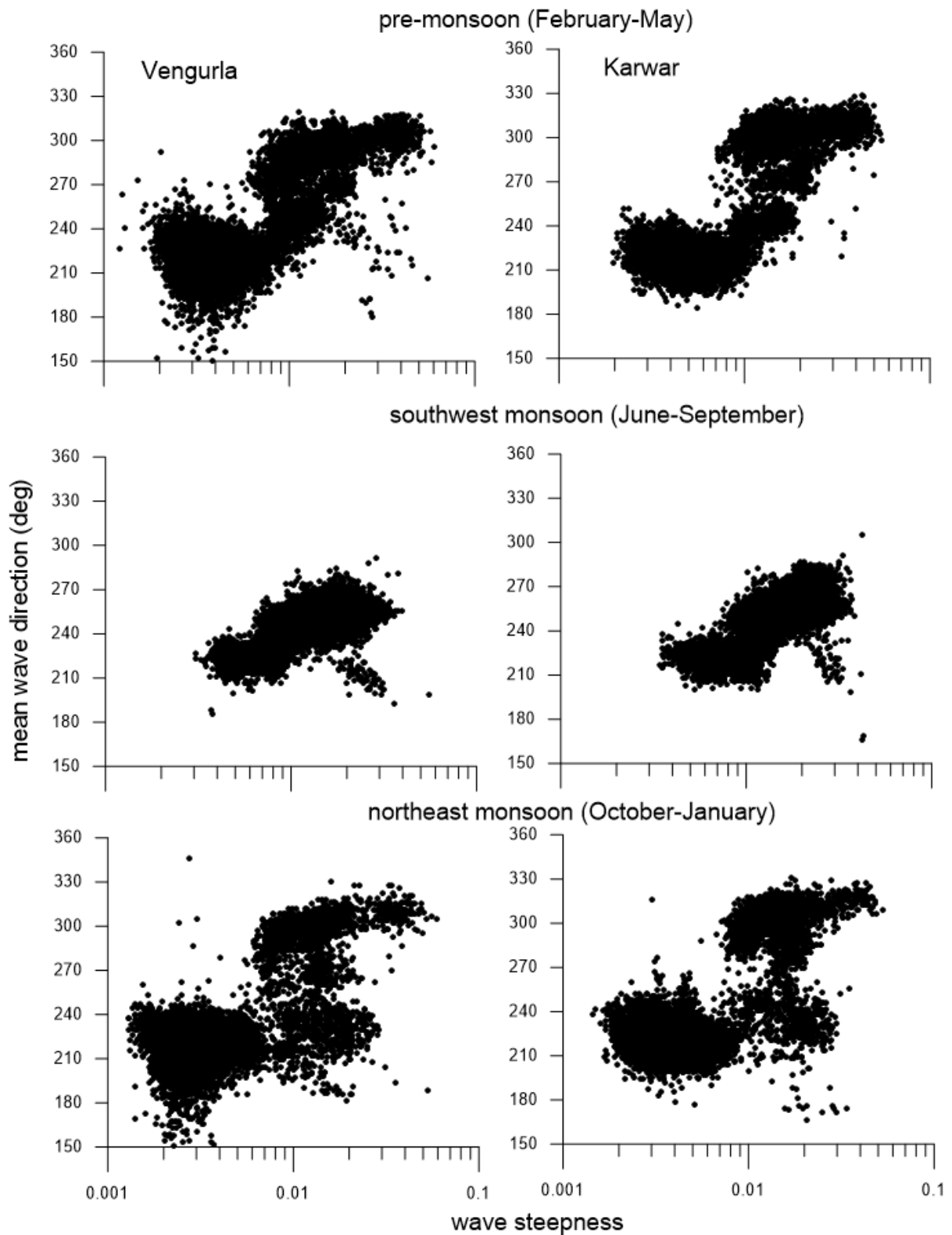


Figure 12. Scatter plot of significant wave steepness with mean wave direction in different seasons. Left side plots are for Vengurla and the right side ones are for Karwar

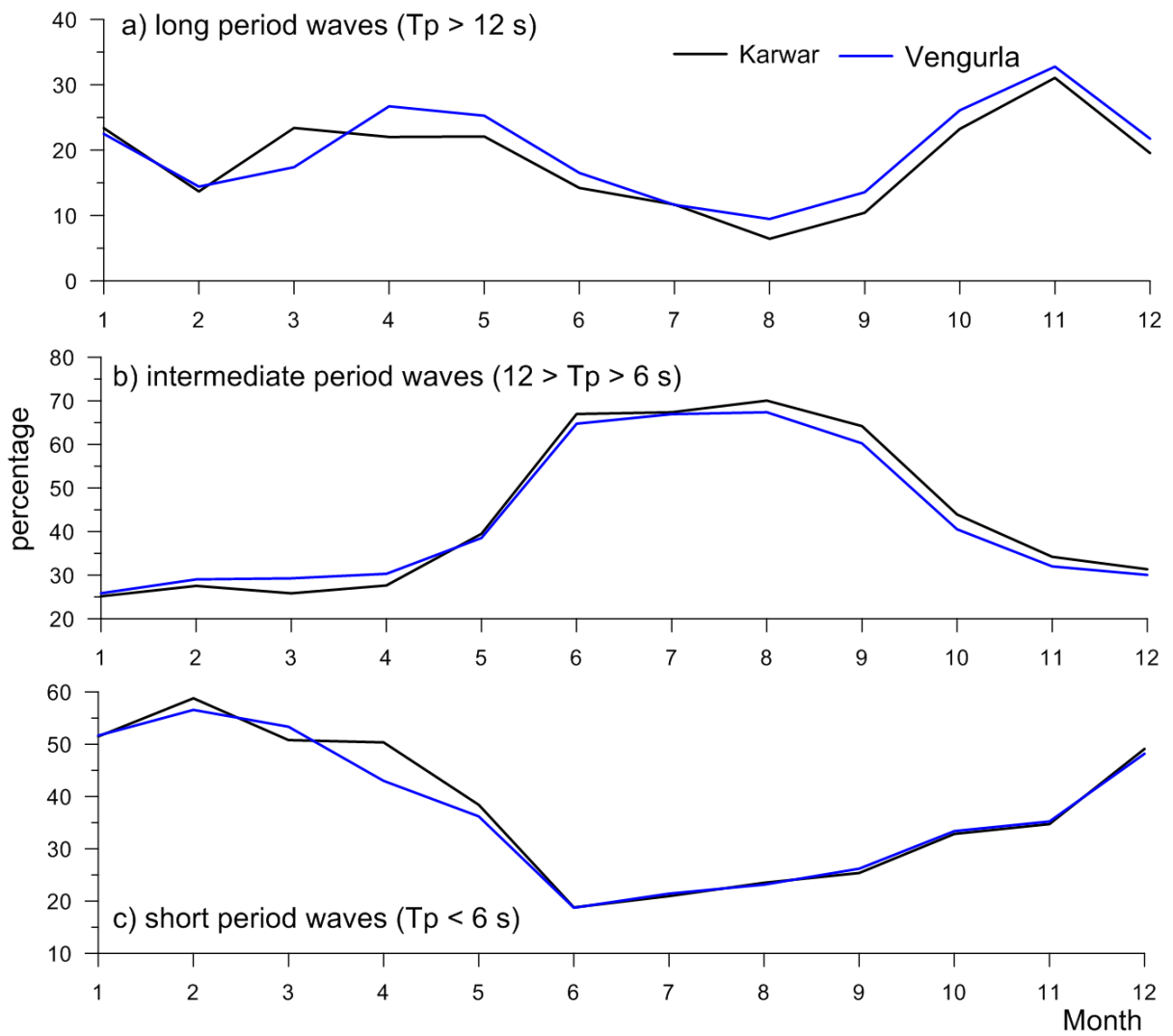


Figure 13. Percentage of long-period, intermediate-period and short-period waves in different months at Vengurla and Karwar. The data presented is the average for 3 years (2015 to 2017)

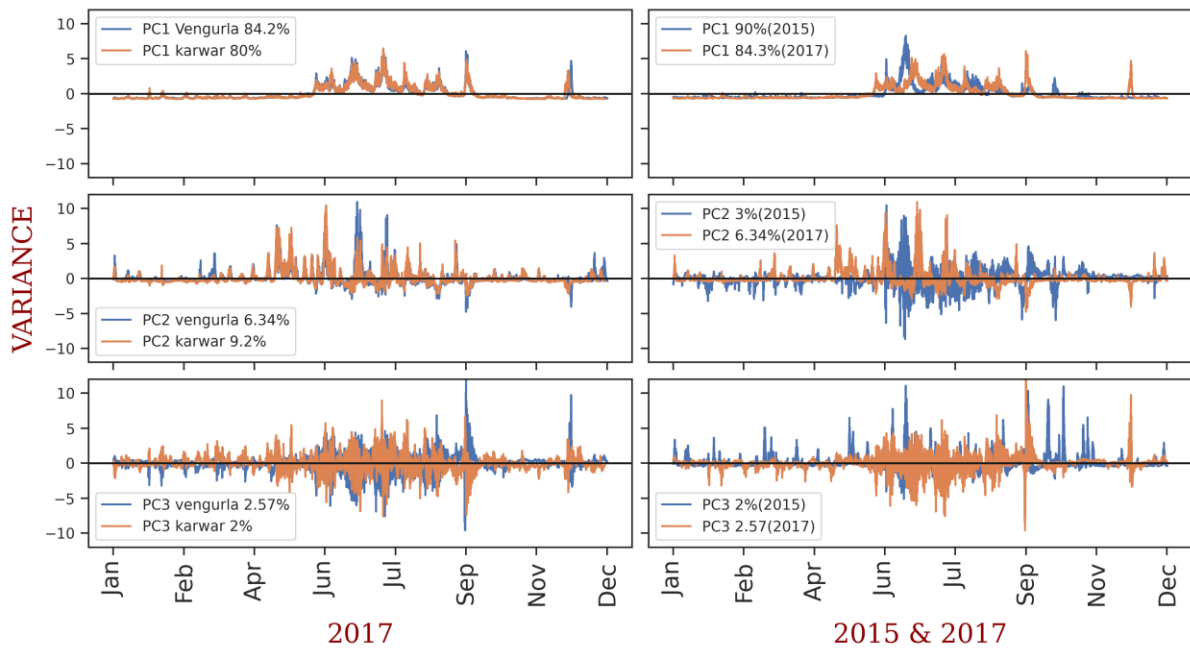


Figure 14. Left panel is the first 3 modes of Principal component of spectral energy density (half-hourly) at Vengurla (Black) and Karwar (Red) in 2017. Right panel is the first 3 modes Principal component (half-hourly) of Vengurla of the year 2015 (Black) and 2017 (Red)

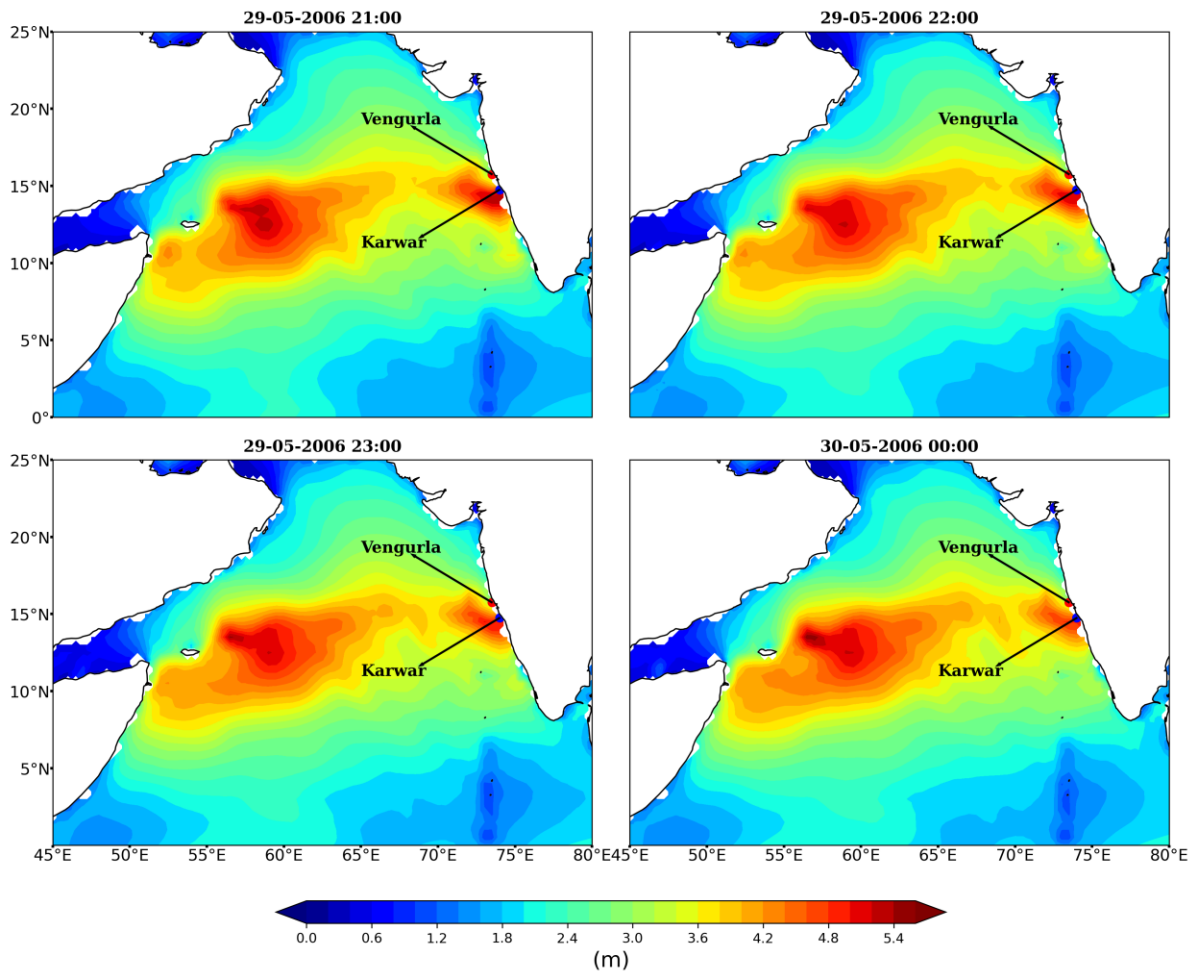


Figure 15. Snapshot of significant wave height from 29 May 2006 2100 hrs to 30 May 2006 0000 hrs based on ERA5 data

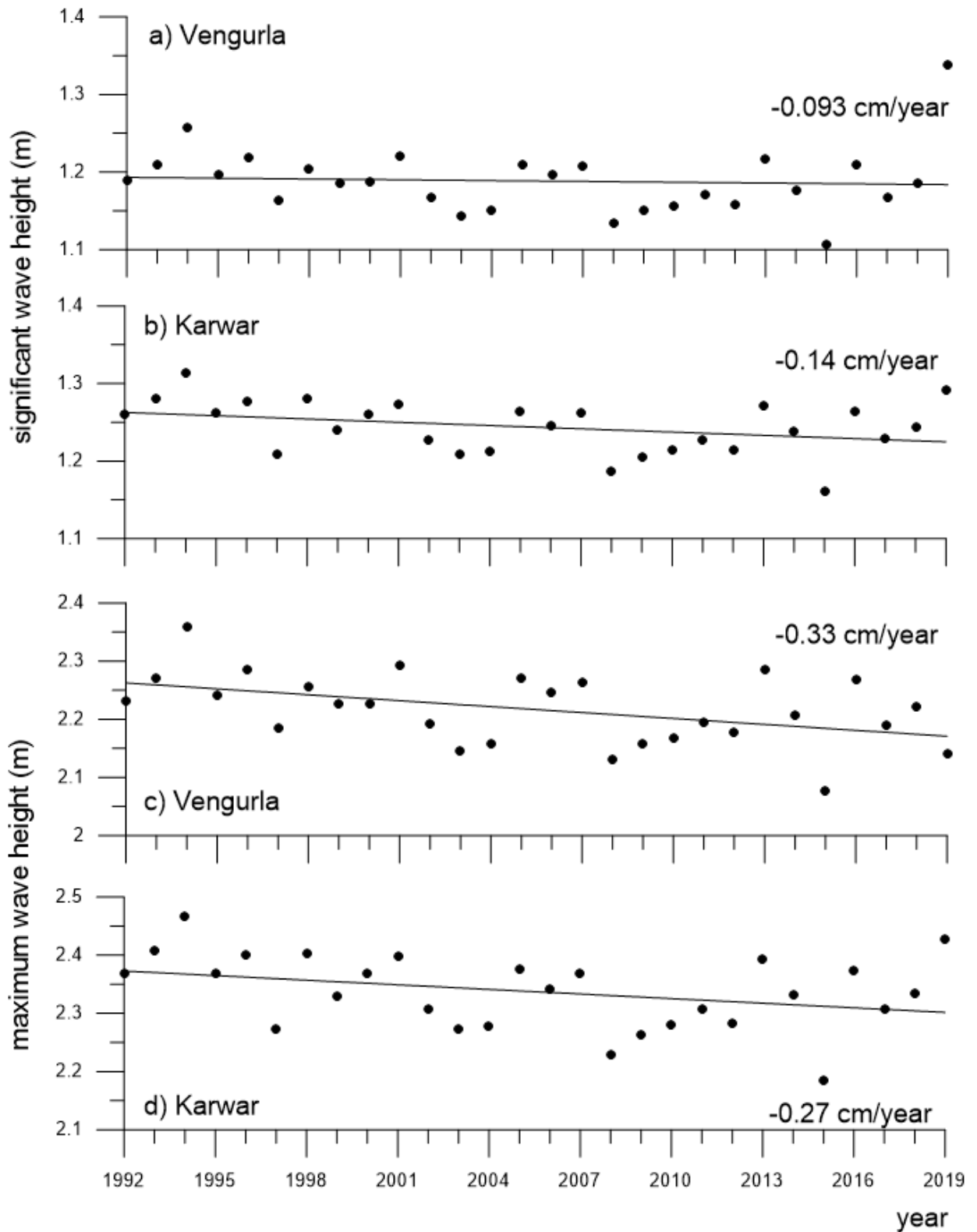


Figure 16. Time series of annual mean significant wave height and maximum wave height as a function of year at Vengurla and Karwar. The long-term trend is also shown in the figure.